Spacecraft Anomaly Forecasting Using Non-Local Environment Data

Jian-Guo Wu, Henrik Lundstedt,
Lars Eliasson, Laila Andersson, Olle Norberg

IRF Scientific Report 263

October 1999

ISSN 0284-1703

Institutet för rymdfysik

Swedish Institute of Space Physics

Kiruna, Sweden

Spacecraft Anomaly Forecasting Using Non-Local Environment Data

Jian-Guo Wu, Henrik Lundstedt,
Lars Eliasson, Laila Andersson, Olle Norberg

IRF Scientific Report 263
October 1999

Institutet för rymdfysik
Swedish Institute of Space Physics

Kiruna, Sweden

IRF Scientific Report 263
ISSN 0284-1703

Swedish Institute of Space Physics
Box 812
SE-981 28 Kiruna
SWEDEN
www.irf.se

STUDY OF PLASMA AND ENERGETIC ELECTRON ENVIRONMENT AND EFFECTS

ESTEC/Contract No. 11974/96/NL/JG(SC)

99-10-27

TECHNICAL NOTE, WP 220

SPACECRAFT ANOMALY FORECASTING USING NON-LOCAL ENVIRONMENT DATA

Authors

Jian-Guo Wu*, Henrik Lundstedt

Swedish Institute of Space Physics, Solar-Terrestrial Physics Division, Scheelevägen 17, SE-223 70 Lund, Sweden.

Lars Eliasson, Laila Andersson, Olle Norberg

Swedish Institute of Space Physics, Box 812, SE-981 28 Kiruna, Sweden

* Now at Danish Meteorological Institute

Lyngbyvej 100, DK-2100 Copenhagen O, Denmark

ESA Technical Officer:
A. Hilgers, Space Environments and Effects Analysis Section (TOS-EMA)

ESA Technological Research Programme
Space Environments and Effects Major Axis

Page left free intentionally

TABLE OF CONTENTS

DOCUMENTATION CHANGE RECORD

Issue	Rev.	Sect.	Date	Comment
Draft	0.1	All	970903	First draft for mid-term review
	0.2	All	980321	Version presented at PM5
	0.3	All	980517	Version presented at PM6
	1.0	All	980529	Version submitted to ESTEC for approval
Final	1.1	All	990103	Revised version
	1.2	All	991027	Second revision mainly editorial

Abstract

In this study, first we construct a space environment database for studies on anomalies on the two geostationary spacecraft, ESA meteorological satellite Meteosat-3 and Swedish telecommunication satellite Tele-X. Second, we investigate through superposed epoch analysis how the two geostationary spacecraft are affected by space environment conditions which are characterised by daily-averaged Dst, daily sum of Kp, and daily-averaged relativistic electron flux (> 2 MeV). Third, we develop neural network models to forecast spacecraft anomalies one day in advance on the basis of experience learned from another spacecraft.

From superposed epoch analysis we find:

- that the spacecraft anomalies frequently occurred during the recovery phase of geomagnetic storms;
- that the space environment during the last 4-6 days preceding an anomaly contributes statistically the most to the anomaly occurrence;
- that Kp and Dst are better correlated with anomalies on Meteosat-3 than the relativistic electron flux (> 2 MeV) to, suggesting that the anomalies on Meteosat-3 were mainly caused by electrons with energy well below 2 MeV (several keV to 300 keV) via, e.g., surface charging or internal charging;
- that the relativistic electron flux is as well correlated with anomalies on Tele-X as Kp and Dst, electrons with energy above 2 MeV (causing internal charging) play a more significant role on Tele-X anomalies than on Meteosat-3 anomalies.

Two neural network paradigms, time delay neural networks and learning vector quantization networks, are exploited in the study. Neural networks are trained only on Meteosat-3 and generalised on both Meteosat-3 and Tele-X. The two network paradigms give consistent prediction results. The prediction results are in agreement with the superposed epoch analysis. From the developed time delay neural network models we find that for Meteosat-3 Kp, Dst, and the energetic electron flux give the total prediction rate (for anomalies and non-anomalies) of 79%, 73%, and 62%, respectively. For Tele-X the total prediction rates are 64%, 66%, and 67% from Kp, Dst and energetic electron flux, respectively. The prediction results are in agreement with the superposed epoch analysis. The neural network models developed in this study can be used to forecast days with higher risks for anomalies from ACE solar wind data or near real-time estimate of Kp.

1 Introduction

1.1 Purpose of this document

This document is the final technical report of a subcontract "Spacecraft Anomaly Forecasting Using Non-Local Environment Data" (WP 220) performed under the contract "Study of plasma and energetic electron environment and effects."

1.2 Main objective

The space environment (including atmosphere, plasma, radiation, and micrometeoroid/orbital debris) can adversely affect spacecraft in space. The type of space environment effects depends on the altitude and inclination of a spacecraft orbit. The magnitude of interactions between the space environment and spacecraft varies with local time, season, geomagnetic and solar activity, with magnitude varying from negligible to mission threatening.

In space plasma environment, the charging which leads to a common potential of a spacecraft is not a problem in itself. However, the differences in surface conductivity, conductors and dielectrics will charge to different potentials in a plasma environment. This differential charging may lead to arc discharging between surfaces if the potential difference is large enough. The arc discharging could cause permanent damage to spacecraft subsystems and electromagnetic interference with sensitive electronics [Tribble, 1995]. Charging currents arise not only from the ambient plasma itself, but from photoelectron and secondary electron emission. The currents of photoelectron emission and secondary electron emission are dominant sources of surface charging in geosynchronous orbit because plasma density is much lower and impact energy is higher than in low earth orbit.

In energetic radiation space environment (including energetic radiation belt particles, cosmic rays, solar protons), the total dose of radiation deposited over the life of the material and the dose rate are the two most important factors responsible for radiation damage. Energetic electrons ($\geq$ 100 keV) are not confined to interact with spacecraft surfaces and will penetrate the surface material into a spacecraft interior and deposit their energy. The amount of energy deposited in a material depends on the type of radiation and its energy as well as the material susceptibility. This will determine the time scale of the internal build-up of charges (internal and deep dielectric charging) for a hazardous electrostatic discharging (dielectric breakdown, gaseous arc discharge) to occur. The time scale may vary from many hours to several days [Vampola, 1994]. Cosmic rays and energetic solar protons can trigger single event effects (e.g., upsets, latch-up) on spacecraft [Wrenn, 1995].

During geomagnetic quiet times, geosynchronous satellites traverse the plasmasphere and are generally earthward of the plasma sheet, and the cold plasmasphere clamps the spacecraft potential at low level. During a typical substorm, a geosynchronous satellite will pass by the inner edge of the plasma sheet and observe the injection of ring current plasma, surface charging can therefore be enhanced due to the injection of hot plasma. During extended intervals of geomagnetic activity and major magnetic storms, high energetic electron fluxes develop on the outer magnetosphere, geosynchronous satellites are generally immersed in the energetic electron environment. These penetrating electrons can become embedded within dielectrics on satellites building up electric fields over time which can exceed the breakdown level of the dielectric [Vampola, 1987].

Geomagnetic storms affect spacecraft through enhanced electron fluxes. Energetic electron flux at the geosynchronous orbit is extremely dynamic, with variation of several orders of magnitude during a few days. Regarding how energetic electron flux depends on geomagnetic activity, it was shown by Nagai [1988], and Koons and Gorney [1991] that the enhancement of electron flux can extend from 1 to 5 days following the storm onset (as measured by Dst and Kp).

All spacecraft are influenced by the space environment but proper design and management can prevent or minimize most of the "space weather" effects. Our work is intended to improve the current knowledge on how the environment influences spacecraft, primarily in geostationary orbit. It is focused on the possibility to predict an anomaly on a spacecraft using non-local environment data from different observatories in space and on the Earth's surface. Another document describes the possibilities to use on-board measurements for forecasting anomalies.

With new sensitive electronic components and low-mass constraints (less shielding) the influence on satellites by the space environment will increase. The possibility to predict times with higher risk for anomalies will be very important also in the future.

In this study, we investigate how the space environment (characterised by energetic electron flux (> 2 MeV) and geomagnetic activity indices Kp and Dst) affects the two geostationary satellites, an ESA meteorological satellite Meteosat-3 and a Swedish telecommunication satellite Tele-X. First we construct the space environment database for the study of 900 anomalies and 560 non-anomalies on the two satellites. Second we make the superposed epoch analysis on the database constructed. Third we develop global neural network models to predict spacecraft anomalies 1 day ahead from the space environment database, without taking local environment conditions into account. Two neural network paradigms are used in this study, i.e., time-delay neural network and learning vector quantization network.

2 Description of data

2.1 Meteosat-3 anomalies

Meteosat-3 was launched on 15 June 1988 as one of the geostationary satellites in the ESA meteorological series. The Eumetsat organisation was operating the satellite. During the lifetime Meteosat-3 was moved several times (see Table 1).

In May 1995 Eumetsat decided that the satellite was not needed but kept it as a reserve around 70° W before finally moving it into junk orbit on 21 November 1995. The anomaly set covers the time period 21 June 1988 to 20 October 1995.

Table 1. *Position of Meteosat-3*

Start of manoeuvre	End	Position
15 June 1988 (launch)	June 1989	0° E
June 1989	January 1990	50° W
January 1990	April 1990	0° E
April 1990	Nov 1990	5° W
July 1991		50° W
late 1992		75° W
April 1993		72.8° W
February 1995	November 1995	70° W and inclined

The most common anomaly on Meteosat-3 occurred in the radiometer, 70 % of all anomalies. The radiometer is located in the middle of the satellite. The total number of anomalies during the mission lifetime was 724. The different types of anomalies are given in Table 2.

Table 2. *Meteosat-3 anomalies*

Code	Description	Number of anomalies
1	Radiometer stops	295
2	Radiometer position jump	84
3	Radiometer position jump and stop	127
4	Other radiometer anomalies	3
5	Battery charger 1 anomaly	7
6	Battery charger 2 anomaly	49
7	Battery charger 1 and/or 2 off	14
8	Battery charger rate anomaly	4

9	Digital multiplexer 1 off / 2 on	8
10	Corrupted/lost image lines	67
11	Command decoder anomaly	3
12	Temperature reading anomaly	14
13	SIC anomaly	29
14	EDA bias jump, SIC lid jump, rad. gain	5
15	VIS 2 gain jump	2
16	Regulator loop voltage anomaly	2
17	Spurious memory reconfiguration	2
18	Other anomalies	9

2.2 Tele-X anomalies

The Tele-X satellite is a broadcasting satellite owned by Nordiska Satellitaktiebolaget, NSAB. It was launched on 2 April 1989 into a geostationary orbit 5°E, inclined and put into junk orbit 1998. Anomalies were registered from the 2 April 1989 (launch) until the end of the mission.

The satellite is a 3-axis stabilised platform with a solar array span of 19 m. The payload mass is 170 kg.

The environment condition considered for the design of Tele-X were: ground handling tests, launcher environment, vibrations and electromagnetic radiation, space radiation, sun incidence angles and eclipses. The considered radiation elements were: electrons trapped in the van Allen belts, low energy protons, high energy protons from solar flares, coronal mass ejections, and cosmic rays.

The calculated radiation dose for different parts was estimated to a maximum value of 1×10^7 rad for sensitive equipment. Externally mounted equipment could be exposed to 5×10^7 rad.

During the period 2 April 1989 to 26 October 1996 192 anomalies were reported (Table 3). Most anomalies are from the Command Manager Unit (CMU) causing the command counter to reset to zero (codes 1-3). Some anomalies were causing a latch valve to spontaneously close (code 4-5). Two anomalies caused a heater to spontaneously heat to higher temperatures than intended (code 6). The on-board computer (OBC) "hanged" (code 7, 8) during the satellite lifetime, and finally contact have been lost between the OBC and the Interface Safety Electronics (ISE) (code 9-10).

Table 3. *Anomalies on Tele-X*

Code	Description	Count
1	CMU1 reset	132
2	CMU2 reset	13
3	CMU1 and CMU2 both reset	8
4	Closure of LV31/41	16
5	Closure of LV32/42	3
6	Spontaneous heater boost	2
7	OBC1 stop	14
8	OBC2 stop	2
9	OBC1/ISE1 data transfer failure	1
10	OBC2/ISE2 data transfer failure	1

2.3 Occurrence of anomalies and non-anomalies on Meteosat-3 and Tele-X

The occurrence of anomalies on Meteosat-3 and Tele-X is compared in Figure 1(d), for 724 anomalies on Meteosat-3 and 192 anomalies on Tele-X. From 21 June 1988 to 20 October 1996 there were 53 days with anomalies on both Meteosat-3 and Tele-X. While only considering the anomalies (on Meteosat-3) included in the training set, from 880621-961020, there were 33 days with anomalies on both Meteosat-3 and Tele-X. There were 26 days in total when anomalies didn't occurred on Tele-X but did occur on Meteosat-3. Here the anomalies on Meteosat-3 refer to those (613 anomalies) used in the neural network study.

In addition, there were 81 data intervals of non-anomalies on Tele-X where anomalies on Meteosat-3 occurred during the last 4 days of the 10 days non-anomaly intervals for Tele-X. This means that 81 non-anomalies on Tele-X were associated with anomalies on Meteosat-3 with the time difference not longer than 4 days. Following the same procedure, but only comparing with the anomalies included in the training set, we obtain that the number of such non-anomalies on Tele-X is 69. These numbers will be useful for post error analysis of the neural network study.

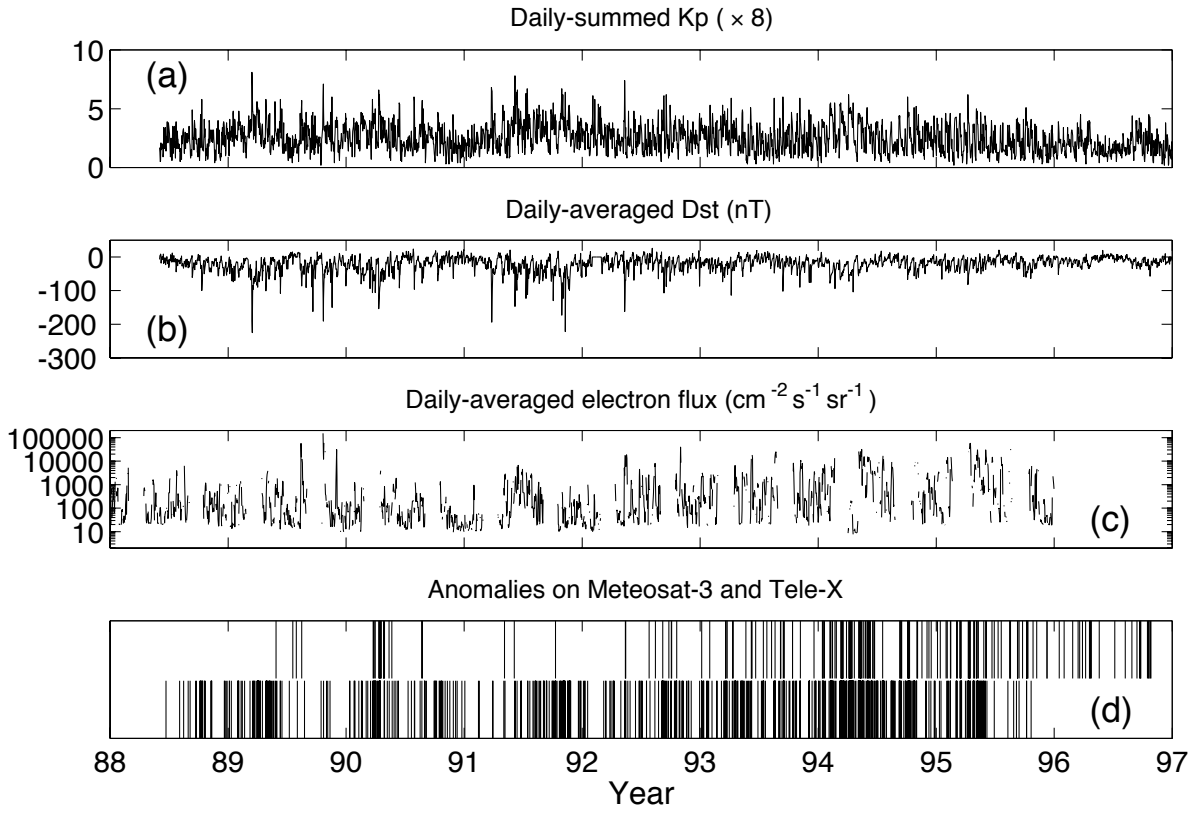

Figure 1. *Anomalies on Meteosat-3 and Tele-X during 880621-961020 and the corresponding space environment conditions. (a) Daily-summed Kp; (b) Daily-averaged Dst (nT); (c) Daily-averaged energetic electron flux with energy above* 2 MeV (cm^{-2} s^{-1} sr^{-1})*, inferred from GOES-7 measurements; and (d) Anomalies on Meteosat-3 (shown in the lower part) and on Tele-X (shown in the upper part).*

2.4 Space environment data

A variety of indices have been utilized to characterize geomagnetic activity. Some of them are designed to characterize specific aspects of the total disturbance field, while others are meant to be global, offering a measure of the worldwide level of magnetic disturbances [Mayaud, 1980; Joselyn, 1995]. The 3-hourly K index is quasi-logarithmic number between 0 and 9 by measuring the largest excursion of magnetic field strength on all three magnetometer orthogonal elements. To remove local influences, the local K index inferred from 11 observatories at geomagnetic latitudes between 45° and 63° in both northern and southern hemisphere are combined to produce a relatively global index, Kp [Bartels, 1949]. At these middle latitudes the observed geomagnetic variations are not the predominant influence of only one current system and may have contributions from different magnetospheric current systems. Therefore Kp derived from geomagnetic perturbations at those latitudes gives a

fairly global characterisation of the energy input into the magnetosphere [Menvielle and Berthelier, 1991].

The Dst index, originally devised by Sugiura [1964], is calculated hourly from the H-component recorded at 4 low latitudes magnetic observatories (20°-30° away from the dipole equator and equally spaced in longitude), where both auroral- and equatorial-electrojet effects are minimal. Dst provides a measure of the strength of the ring current (the total energy of ring current particles) and serves as an indicator of the intensity and duration of magnetic storms. Ring current is formed by ions (mainly protons and oxygen ions) and electrons in the 10-300 keV range, where electrons do not contribute much to the ring current energy, but to penetrating radiation. Dst is essentially the value of the ring current at the dipole equator, with some uncertainties due to magnetic contributions from other sources, e.g., magnetopause currents, asymmetric ring current, and substorm current wedge, as discussed by Rostoker [1972].

Kp and Dst indices and energetic electron flux (>2 MeV) are used here as environmental parameters to correlate with spacecraft anomalies. Hourly Dst and 3-hourly Kp data are taken from NSSDC OMNIWeb. Daily-averaged Dst and daily-summed Kp are actually used in this study. The daily-averaged energetic electron flux are inferred from original 5-minute averaged data measured by NOAA GOES-6, GOES-7, and GOES-8. For Kp, we take the daily-summed values since 3-hourly Kp cannot be averaged due to its quasi-logarithmic scale. The choice with daily resolution is mainly due to the fact that Meteosat-3, Tele-X and the GOES satellites are located at different longitudes along the geostationary orbit. The environment data used to study the anomalies on Meteosat-3 and Tele-X are shown in Figures 1(a)-(c).

The data interval for an anomaly is defined as a period of time preceding a day when an anomaly occurred on Meteosat-3 or on Tele-X. The maximal interval selected is 10 days. The data interval for a non-anomaly is defined as a period of time preceding a day when anomalies did not occur on Meteosat-3 or on Tele-X and during the data interval anomalies did not occur on Meteosat-3 or on Tele-X. The maximal interval selected is 10 days as well. Therefore, definitions of an anomaly interval and a non-anomaly interval are satellite-dependent. After data processing (mainly due to the gaps in GOES measurements), we thus obtain 613 data anomaly intervals for Meteosat-3 and 167 anomaly intervals for Tele-X. We obtain 420 data non-anomaly intervals for Meteosat-3 and 140 non-anomaly data intervals for Tele-X.

3 Superposed epoch analysis

The superposed epoch analysis is made on the database constructed above. The results are shown in Figures 2(a)-(c) for Meteosat-3 and Tele-X. As seen from the averaged anomaly interval pattern of Kp or Dst, anomalies tend to occur during the period of time when geomagnetic activity starts decreasing after reaching the maximum. We find the same result for anomalies on both Meteosat-3 and Tele-X. This indicates that the spacecraft anomalies frequently occurred during the recovery phase of geomagnetic storms. Furthermore, the space environment conditions during the last 4-6 days preceding an anomaly are seen to contribute statistically the most to the occurrence of anomalies on both Meteosat-3 and Tele-X. Those results are consistent with the fact that geomagnetic storms affect spacecraft through enhanced electron fluxes (with a delay from 1 to 5 days following the storm onset). The main phase generally lasts about 1 day, electron fluxes are therefore enhanced during the recovery phase of magnetic storms.

As seen from Figure 2, for Meteosat-3 the patterns of Kp or Dst for the averaged data interval of anomalies and non-anomalies are more clearly distinguished from each other than energetic electron flux (>2 MeV). This means that Kp and Dst would be better input parameters than the energetic electron flux in predicting anomalies on Meteosat-3. This also suggests that the anomalies on Meteosat-3 mainly involve electrons with energy in the range 10-300 keV. This energy range can lead to surface charging or internal charging.

In contrast, for Tele-X the averaged anomaly interval and the averaged non-anomaly interval for energetic electron fluxes are also clearly distinguished from each other as those for Dst and Kp. This means that the energetic electron flux would be a parameter as good as Kp and Dst in predicting anomalies on Tele-X, thereby suggesting that the majority of the anomalies on Tele-X significantly involve electrons with energy above 2 MeV and therefore could be due to internal charging.

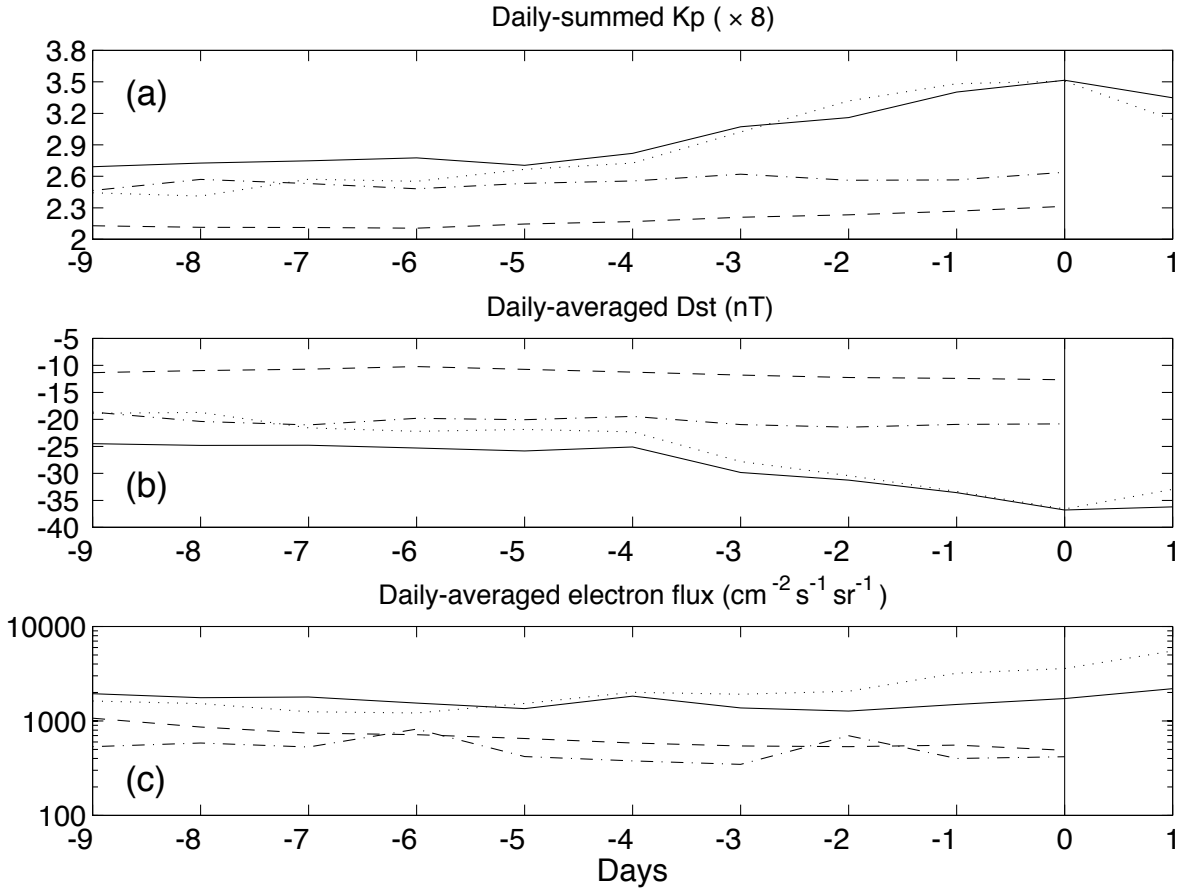

Figure 2. *Superposed epoch analysis on anomaly and non-anomaly data intervals characterised by space environment parameters: (a) Daily-summed Kp; (b) Daily-averaged Dst (nT); (c) Daily-averaged energetic electron flux with energy above* 2 MeV *($cm^{-2}s^{-1}sr^{-1}$). The solid line represents the mean distribution of anomaly intervals averaged for 691 anomalies on Meteosat-3 and the dashed line represents the mean distribution of non-anomaly intervals averaged for 420 non-anomalies on Meteosat-3. The dotted line refers to the mean distribution of anomaly intervals averaged for 167 anomalies on Tele-X and the dashed-dotted line to the mean distribution of non-anomaly intervals averaged for 140 non-anomalies on Tele-X.*

4 Prediction of anomalies using neural networks

Neural networks (NNs) have been successfully applied in study of solar wind-magnetosphere coupling [Wu and Lundstedt, 1996, 1997a, 1997b]. With WIND solar wind plasma and interplanetary magnetic field data as input, the validity of developed NN models has further been verified from their capability to accurately predict a major magnetic storm triggered by the 1997 January halo-CME [Wu et al., 1998]. The resulting enhancement of relativistic electron fluxes in the magnetosphere was suspected as the killer of AT&T Telstar 401 satellite on January 11, 1997. NNs have also been exploited in spacecraft anomaly analysis and predictions [Lòpez and Hilgers, 1997; Wu et al., 1998b].

On the basis of the above superposed epoch analysis, we further develop global NN models to predict spacecraft anomalies 1 day ahead from the space environment database. Without considering the local conditions. Time-delay NNs with standard gradient descent algorithm and adaptive learning scheme and learning vector quantization NNs [Hertz et al., 1991] are exploited in this study.

A time-delay neural network (TDNN) is a supervised learning feed-forward back-propagation network with a time delay line in the input layer. Learning Vector Quantization (LVQ) is a classification network, which assigns vectors to one of several classes. A LVQ network contains a Kohonen layer that learns and performs the classification. The input layer contains one neuron for each input parameter, the output layer contains one neuron for each class. LVQ network is a combination of supervised and un-supervised learning networks. The classes are predefined and we have a body of labelled sample data; each sample input vector is tagged with its correct class. This is the sense of being supervised. "Un-supervised" in LVQ refers to its way of weight updating.

NNs are trained only on Meteosat-3 and the trained neural network models are generalised on Meteosat-3 and Tele-X. The network output is set to 1 for an anomaly and to 0 for a non-anomaly in the training set. For test, if the output is in the range (0.5, 1.5), then it is classified as an anomaly; If the output is in the range (-0.5, 0.5), it is classified as a non-anomaly; If the output falls outside the 2 ranges, then the output is classified as uncertain.

4.1 Training and test data

Daily averaged energetic electron flux, daily averaged Dst and daily sum of Kp are the input parameter. The data of Dst, Kp and the logarithm of electron flux are linearly normalised to [-1, 1]. The maximum and minimum values of the daily sum of Kp are 8.1 (x 8) and 0.2 (x 8). The maximum and minimum values of the daily Dst are 2.6 nT and -225.0 nT. The maximum and minimum values of the daily electron flux are 2.88×10^5 and 1.00 ($cm^{-2}s^{-1}sr^{-1}$).

Training takes place on 70% of the events (including anomalies and non-anomalies) on Meteosat-3 only. Trained NNs are first generalised from the rest 30% of the events on Meteosat-3 (test set #1) and then tested on Tele-X (test set #2) to see how the trained NN models can generalise from Meteosat-3 to Tele-X. The training set consists of 454 anomalies and 279 non-anomalies on Meteosat-3. The test set #1 consists of 159 anomalies and 131 non-anomalies on Meteosat-3. The test set #2 consists of 167 anomalies and 140 non-anomalies on Tele-X.

4.2 Predictions using time-delay neural networks

We predict anomalies and non-anomalies on the satellites Meteosat-3 and Tele-X one day in advance. In each case we present the prediction results for training and test. The prediction rate for anomalies is defined as the number of correct predictions for anomalies divided by the number of anomalies in a data set. The prediction rate for non-anomalies is defined as the number of correct predictions for non-anomalies divided by the number of non-anomalies in the data set. The total prediction rate is defined as the total number of correct predictions for both anomalies and non-anomalies divided by the total number of anomalies and non-anomalies in the data set.

4.2.1 Case study 1: Input Kp

With Kp as input, the prediction results are summarised in Table 4 and are shown in Figures 3(a)-(i) in terms of different time delay line in the input layer and different number of network hidden neurons.

The quantities in Table 4 are specified here. τ is the length of a time delay line. S is the number of hidden neurons. R_{te} is the total rate of prediction for anomalies and non-anomalies on Meteosat-3. R_{te1} is the rate of prediction for anomalies on Meteosat-3. R_{te2} is the rate of prediction for non-anomalies on Meteosat-3. R_{tlx} is the total rate of prediction for anomalies and non-anomalies on Tele-X. R_{tlx1} is the rate of prediction for anomalies on Tele-X. R_{tlx2} is the rate of prediction for non-anomalies on Tele-X. R_{tr} is the total training rate of prediction for anomalies and non-anomalies on Meteosat-3. R_{tr1} is the training rate of prediction for anomalies on Meteosat-3. R_{tr2} is the training rate of prediction for non-anomalies on Meteosat-3. These quantities are also applied in the following tables.

Let us take one of the best results for 8 days time window as an example. For anomalies on Meteosat-3, Kp can predict 78% correctly while for non-anomalies on Meteosat-3 Kp can predict 80% correctly. The total prediction rate is 79%. For events on Tele-X, Kp gives the total prediction rate 64% where 78% is for anomalies and 46% for non-anomalies.

Table 4. One day ahead prediction of spacecraft anomalies from Kp (TDNN)

$\tau(days)$	S	R_{te}	R_{te1}	R_{te2}	R_{tlx}	R_{tlx1}	R_{tlx2}	R_{tr}	R_{tr1}	R_{tr2}
4	4	0.723	0.786	0.652	0.664	0.826	0.471	0.750	0.815	0.645
4	8	0.730	0.767	0.688	0.681	0.844	0.486	0.735	0.811	0.613
4	12	0.723	0.780	0.660	0.671	0.832	0.479	0.742	0.815	0.624
4	16	0.743	0.761	0.723	0.681	0.820	0.514	0.731	0.795	0.627
4	20	0.740	0.799	0.674	0.658	0.826	0.457	0.744	0.826	0.609
6	4	0.710	0.748	0.667	0.638	0.814	0.429	0.756	0.815	0.659
6	8	0.713	0.761	0.660	0.645	0.844	0.407	0.759	0.828	0.645
6	12	0.733	0.748	0.716	0.664	0.808	0.493	0.759	0.795	0.699
6	16	0.720	0.774	0.660	0.638	0.814	0.429	0.748	0.819	0.631
6	20	0.700	0.742	0.652	0.632	0.826	0.400	0.763	0.837	0.642
8	4	0.750	0.774	0.723	0.648	0.784	0.486	0.754	0.811	0.663
8	8	0.790	0.780	0.801	0.635	0.784	0.457	0.753	0.813	0.656
8	12	0.763	0.767	0.759	0.638	0.778	0.471	0.769	0.822	0.685
8	16	0.773	0.792	0.752	0.642	0.796	0.457	0.765	0.833	0.656
8	20	0.757	0.774	0.738	0.622	0.802	0.407	0.763	0.841	0.634
10	4	0.733	0.686	0.787	0.606	0.743	0.443	0.783	0.852	0.670
10	8	0.743	0.711	0.780	0.638	0.772	0.479	0.768	0.830	0.667
10	12	0.750	0.717	0.787	0.625	0.772	0.450	0.769	0.837	0.659
10	16	0.747	0.736	0.759	0.635	0.814	0.421	0.767	0.852	0.627
10	20	0.767	0.748	0.787	0.619	0.766	0.443	0.771	0.833	0.670

(a)

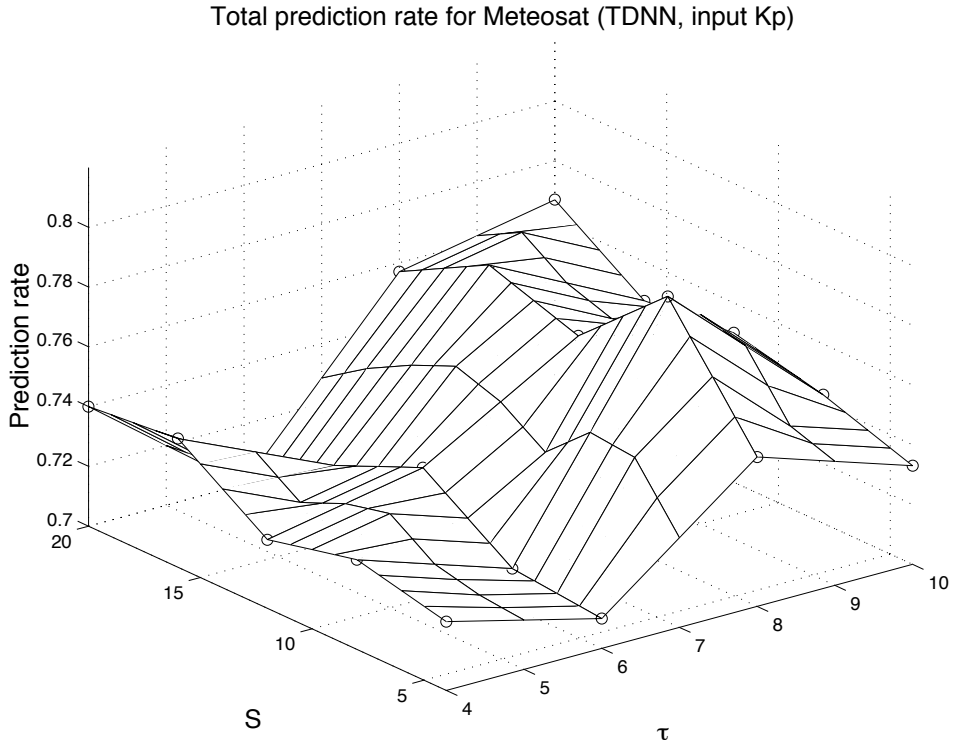
Total prediction rate for Meteosat (TDNN, input Kp)
Prediction rate
0.8
0.78
0.76
0.74
0.72
0.7
20
15
10
5
S
4
5
6
7
8
9
10
τ

(b)

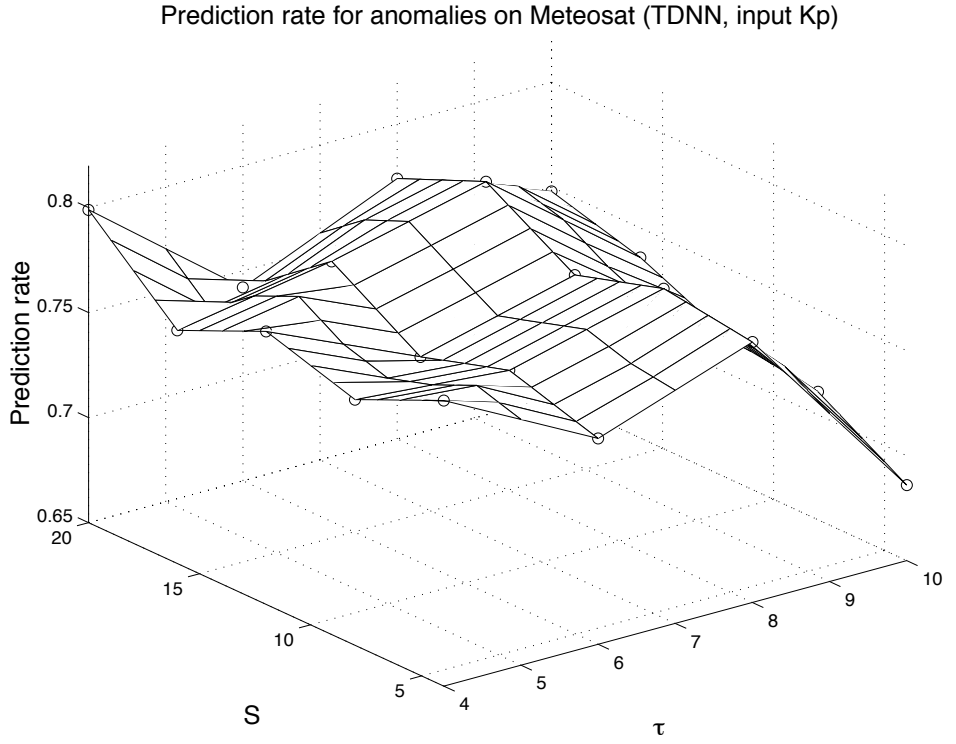
Prediction rate for anomalies on Meteosat (TDNN, input Kp)
Prediction rate
0.8
0.75
0.7
0.65
20
15
10
5
S
4
5
6
7
8
9
10
τ

(c)

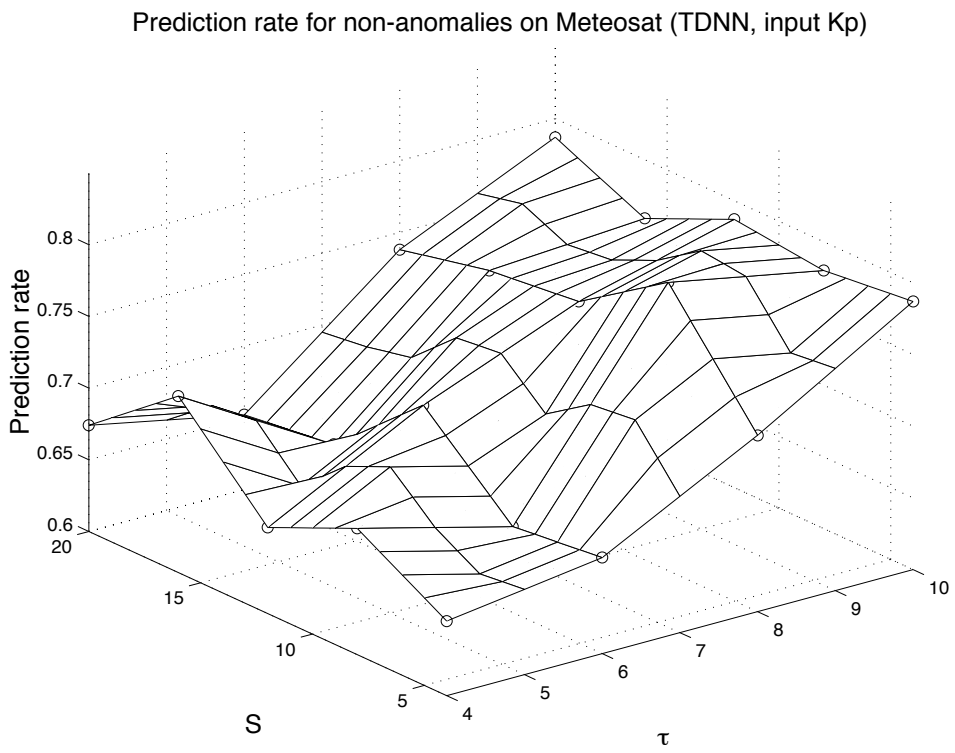
Prediction rate for non-anomalies on Meteosat (TDNN, input Kp)
Prediction rate
0.8
0.75
0.7
0.65
0.6
20
15
10
5
S
4
5
6
7
8
9
10
τ

(d)

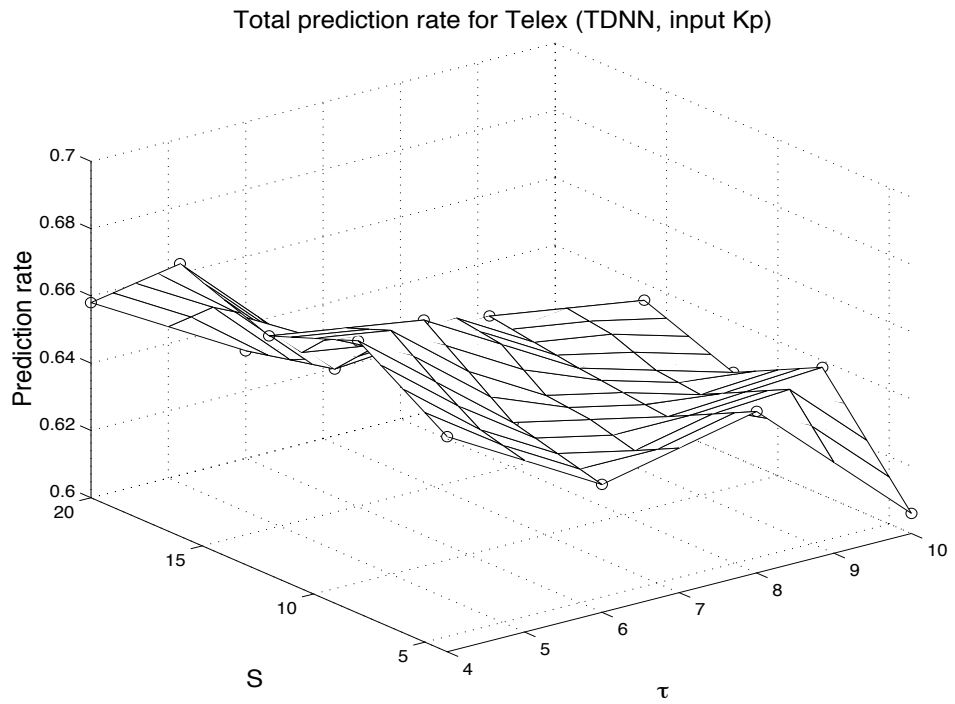
Total prediction rate for Telex (TDNN, input Kp)
Prediction rate
0.7
0.68
0.66
0.64
0.62
0.6
20
15
10
5
S
4
5
6
7
8
9
10
τ

(e)

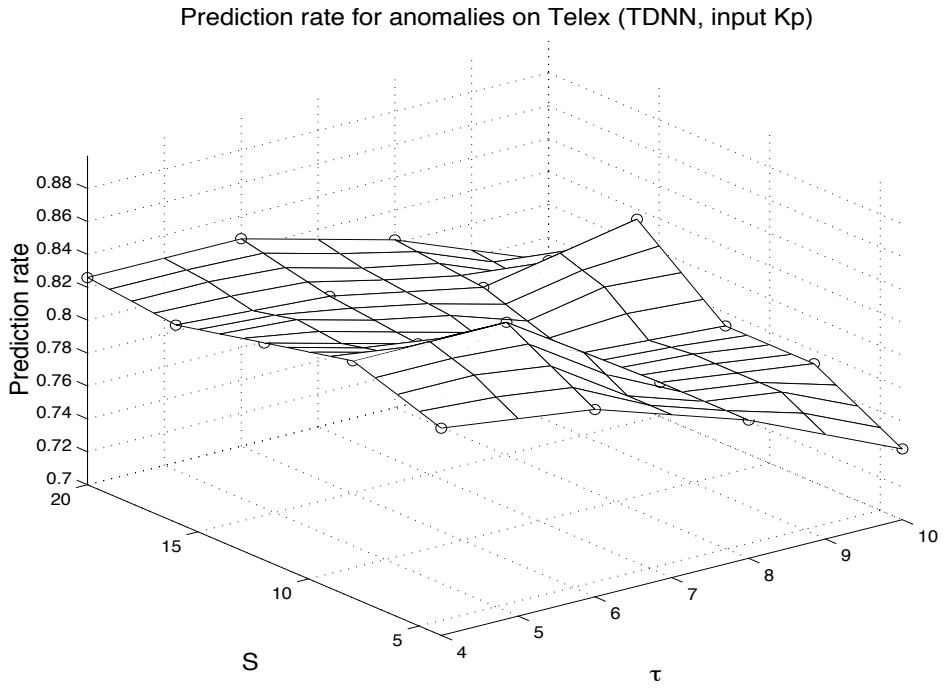
Prediction rate for anomalies on Telex (TDNN, input Kp)
Prediction rate
0.88
0.86
0.84
0.82
0.8
0.78
0.76
0.74
0.72
0.7
20
15
10
5
S
4
5
6
7
8
9
10
τ

(f)

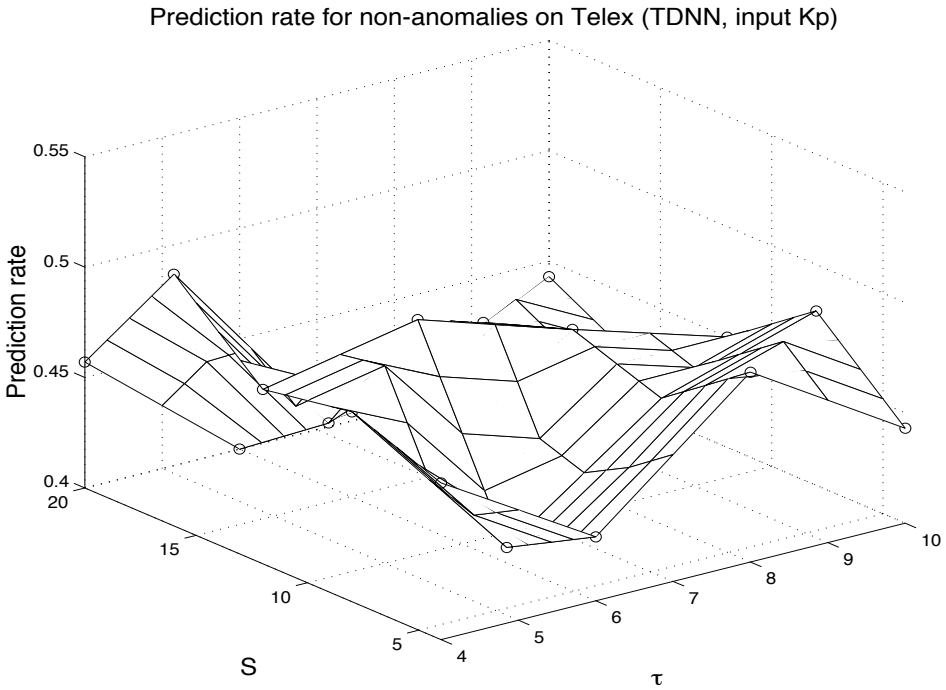
Prediction rate for non-anomalies on Telex (TDNN, input Kp)
Prediction rate
0.55
0.5
0.45
0.4
20
15
10
5
S
4
5
6
7
8
9
10
τ

(g)

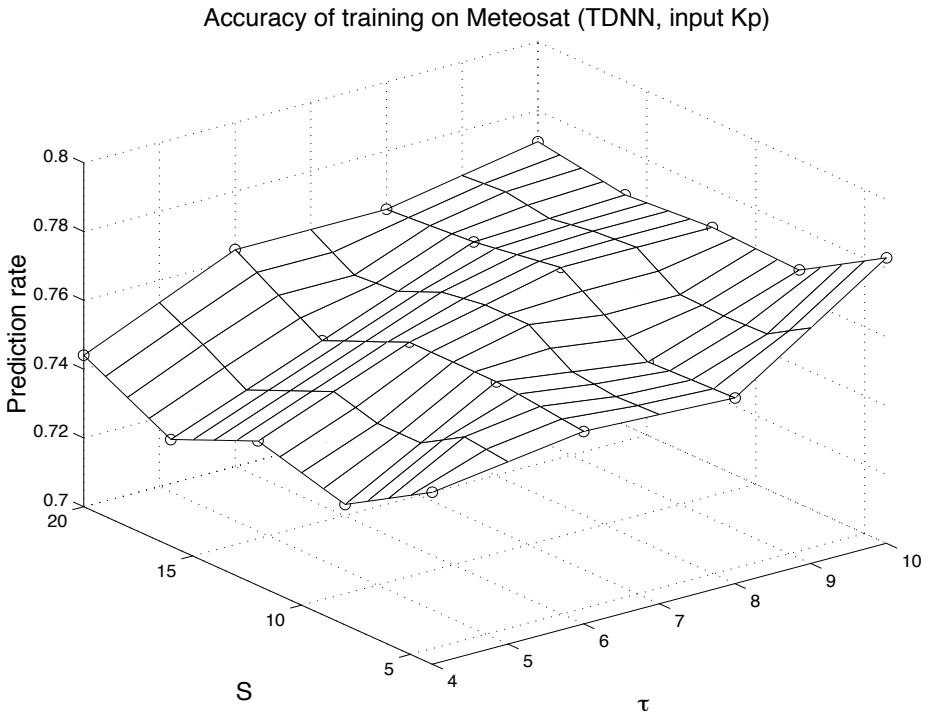
Accuracy of training on Meteosat (TDNN, input Kp)
Prediction rate
0.8
0.78
0.76
0.74
0.72
0.7
20
15
10
5
S
4
5
6
7
8
9
10
τ

(h)

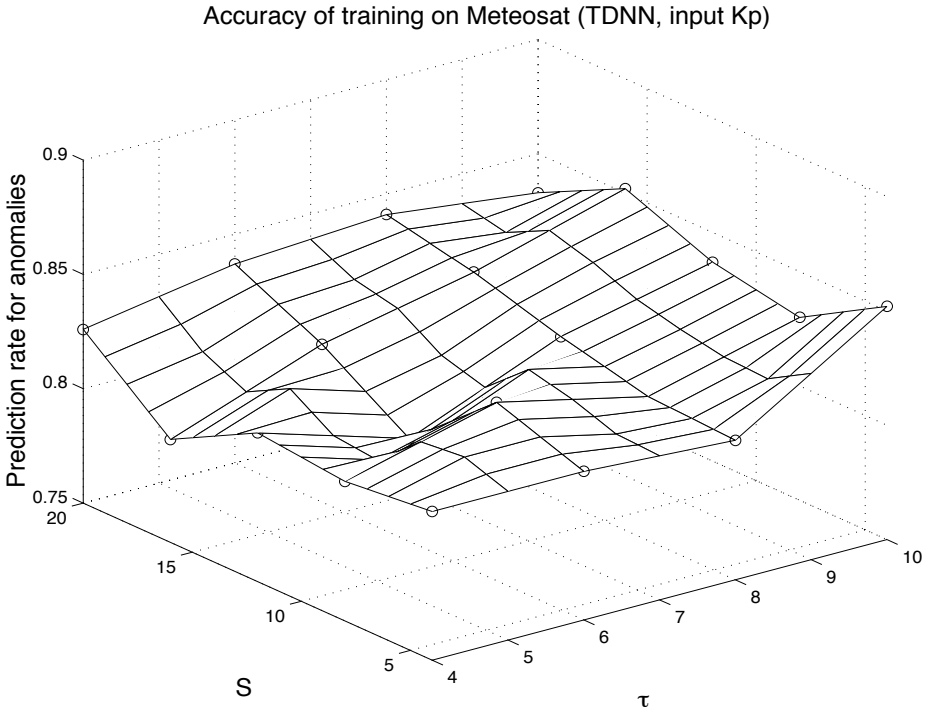
Accuracy of training on Meteosat (TDNN, input Kp)
Prediction rate for anomalies
0.9
0.85
0.8
0.75
20
15
10
5
S
4
5
6
7
8
9
10
τ

(i)

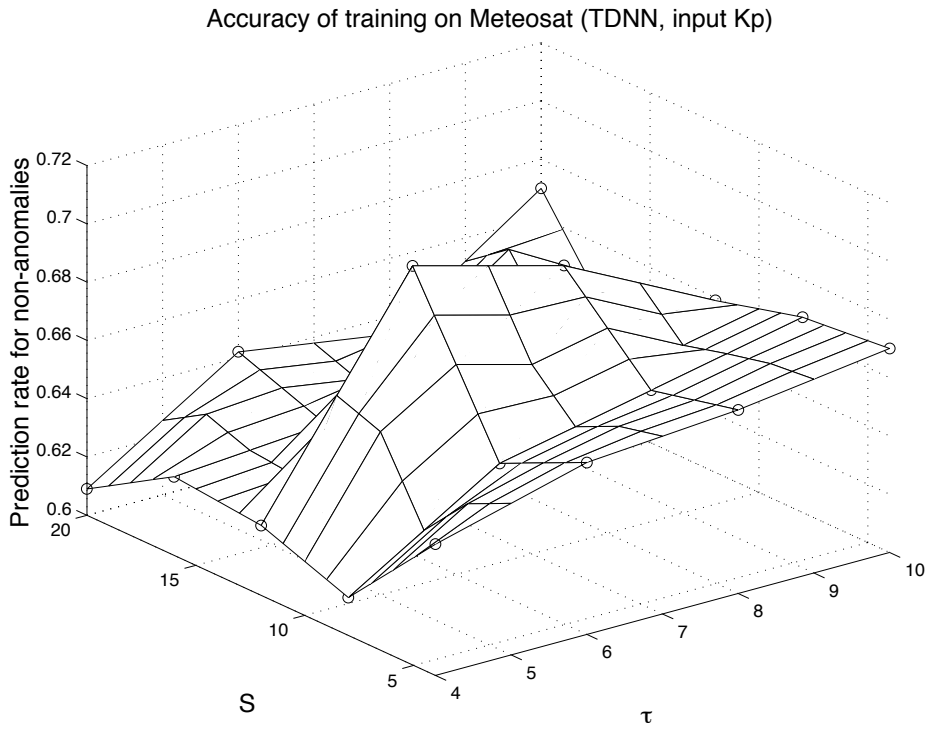

Figure 3. *Predictions one day ahead from the input Kp using TDNN in terms of the network architecture (i.e., the time delay line and the number of hidden neurons). (a) Total prediction rate for Meteosat-3; (b) Prediction rate for anomalies on Meteosat-3; (c) Prediction rate for non-anomalies on Meteosat-3; (d) Total prediction rate for Tele-X; (e) Prediction rate for anomalies on Tele-X; (f) Prediction rate for non-anomalies on Tele-X; (g) Training accuracy on Meteosat-3; (h) Training accuracy for anomalies on Meteosat-3; (i) Training accuracy for non-anomalies on Meteosat-3;*

As the time delay line varies from 4 to 10 days and the number of network hidden neurons varies from 4 to 20, the total prediction rate varies between 71% and 79% for events on Meteosat-3 and varies between 62% and 68% for events on Tele-X. An 8 days time delay line gives slightly better accuracy than the others using Kp as the input parameter.

In summary, the prediction rate varies between 71% and 80% for anomalies and between 65% and 80% for non-anomalies on Meteosat-3. For Tele-X, the prediction rate varies between 77% and 84% for anomalies and between 40% and 51% for non-anomalies.

4.2.2 Case study 2: Input Dst

The prediction results are given in Table 5 and Figures 4(a)-(i) using Dst as the input parameter. When the delay line length is 8 days, the total prediction rate is 73% for events on Meteosat-3, the prediction rate is 77% for anomalies and 67% for non-anomalies on Meteosat-3. The total prediction rate is 65% for events on Tele-X, the prediction rate is 81% for anomalies and 44% for non-anomalies on Tele-X. The definition of non-anomalies is still

the main reason for that non-anomalies on Tele-X cannot be well predicted. A 10 or 8 days delay line results in similar prediction accuracy.

Table 5. One day ahead prediction of spacecraft anomalies from Dst (TDNN)

$\tau(days)$	S	R_{te}	R_{te1}	R_{te2}	R_{tlx}	R_{tlx1}	R_{tlx2}	R_{tr}	R_{tr1}	R_{tr2}
4	4	0.687	0.799	0.560	0.651	0.844	0.421	0.759	0.826	0.649
4	8	0.693	0.792	0.582	0.651	0.844	0.421	0.757	0.826	0.645
4	12	0.700	0.774	0.617	0.661	0.832	0.457	0.749	0.804	0.659
4	16	0.693	0.792	0.582	0.661	0.844	0.443	0.754	0.819	0.649
4	20	0.690	0.786	0.582	0.651	0.844	0.421	0.761	0.828	0.652
6	4	0.707	0.748	0.660	0.635	0.814	0.421	0.769	0.833	0.667
6	8	0.707	0.748	0.660	0.622	0.802	0.407	0.761	0.830	0.649
6	12	0.707	0.748	0.660	0.625	0.802	0.414	0.764	0.833	0.652
6	16	0.713	0.704	0.723	0.625	0.772	0.450	0.760	0.782	0.724
6	20	0.700	0.730	0.667	0.622	0.790	0.421	0.756	0.815	0.659
8	4	0.720	0.786	0.645	0.651	0.826	0.443	0.772	0.835	0.670
8	8	0.710	0.723	0.695	0.635	0.796	0.443	0.759	0.811	0.674
8	12	0.723	0.780	0.660	0.648	0.832	0.429	0.765	0.828	0.663
8	16	0.727	0.774	0.674	0.645	0.814	0.443	0.768	0.824	0.677
8	20	0.713	0.748	0.674	0.642	0.820	0.429	0.763	0.826	0.659
10	4	0.733	0.748	0.716	0.642	0.808	0.443	0.772	0.828	0.681
10	8	0.730	0.774	0.681	0.658	0.832	0.450	0.778	0.844	0.670
10	12	0.727	0.742	0.709	0.645	0.820	0.436	0.779	0.839	0.681
10	16	0.730	0.761	0.695	0.648	0.826	0.436	0.775	0.844	0.663
10	20	0.720	0.767	0.667	0.655	0.832	0.443	0.778	0.844	0.670

(a)

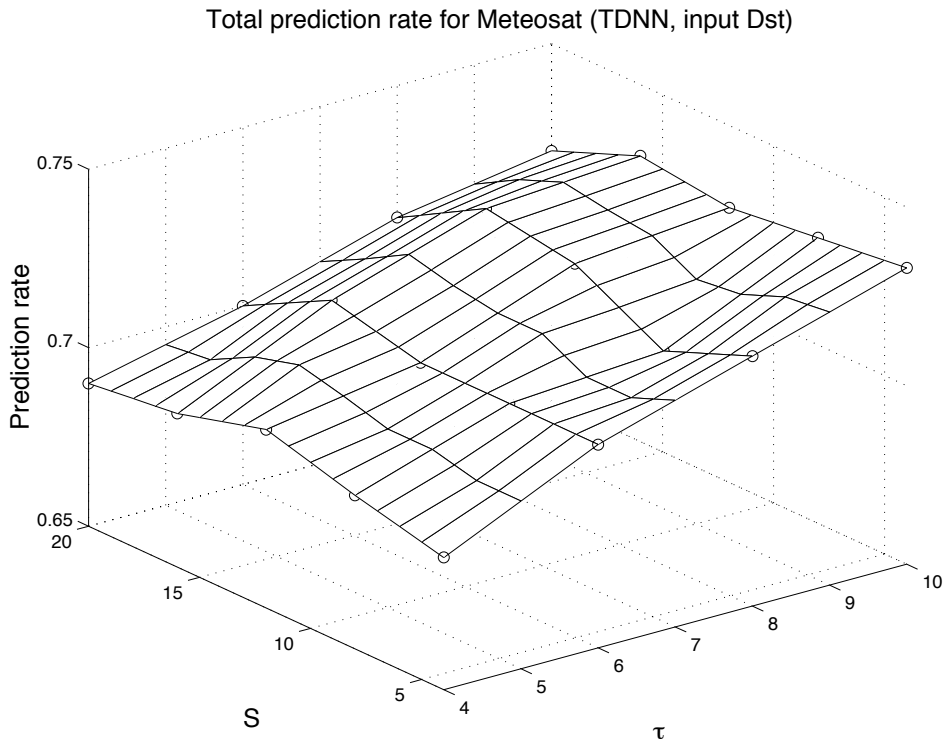
Total prediction rate for Meteosat (TDNN, input Dst)
Prediction rate
0.75
0.7
0.65
20
15
10
5
S
4
5
6
7
8
9
10
τ

(b)

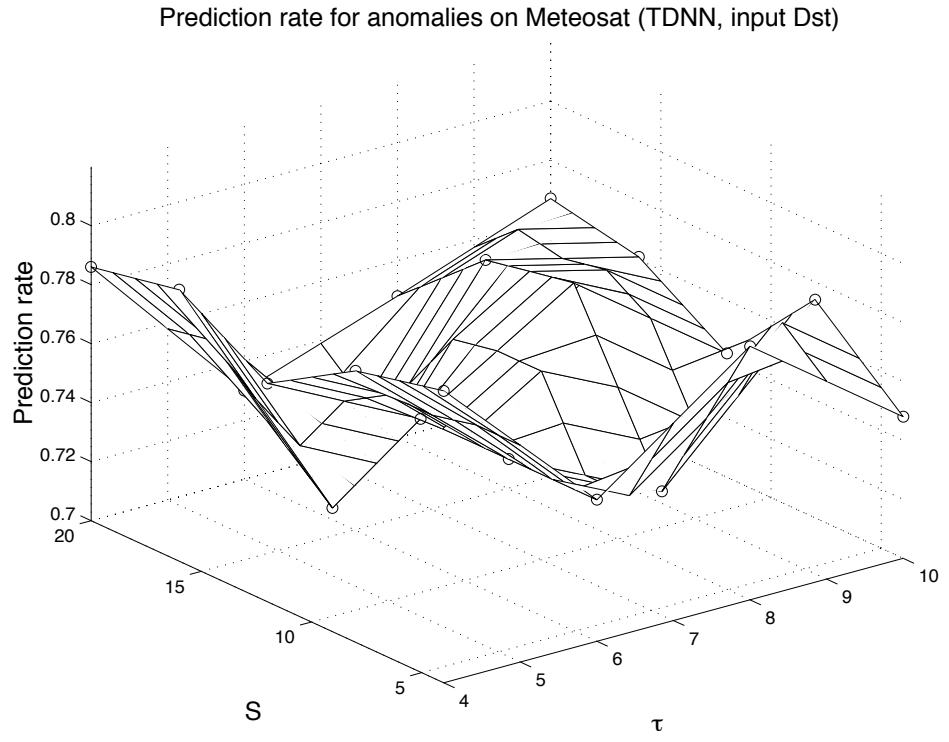
Prediction rate for anomalies on Meteosat (TDNN, input Dst)
Prediction rate
0.8
0.78
0.76
0.74
0.72
0.7
20
15
10
5
S
4
5
6
7
8
9
10
τ

(c)

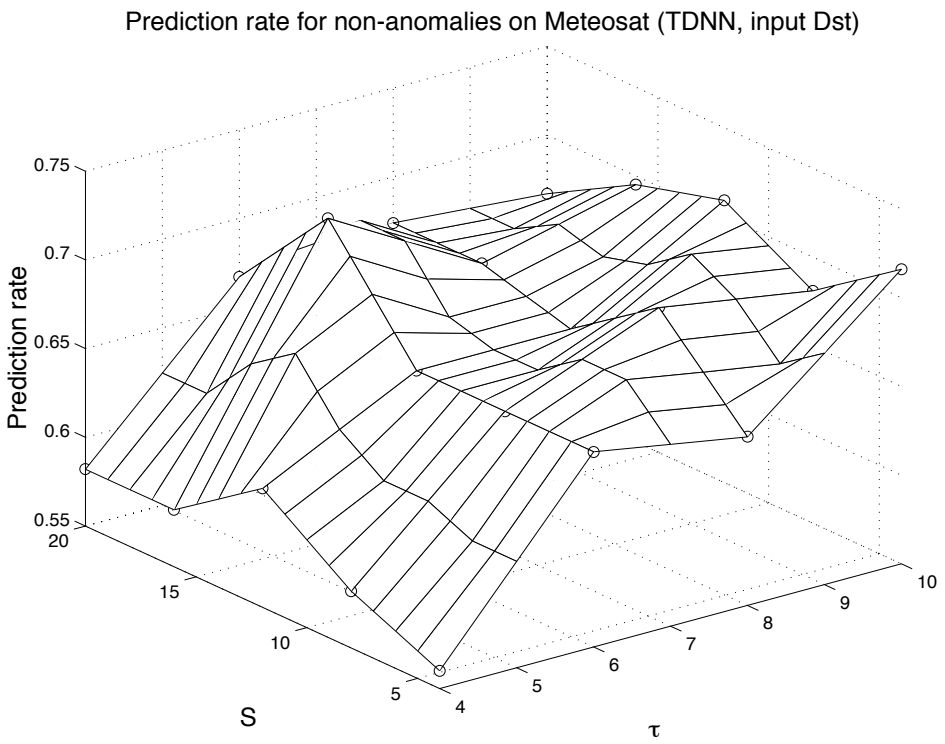
Prediction rate for non-anomalies on Meteosat (TDNN, input Dst)
Prediction rate
0.75
0.7
0.65
0.6
0.55
20
15
10
5
S
4
5
6
7
8
9
10
τ

(d)

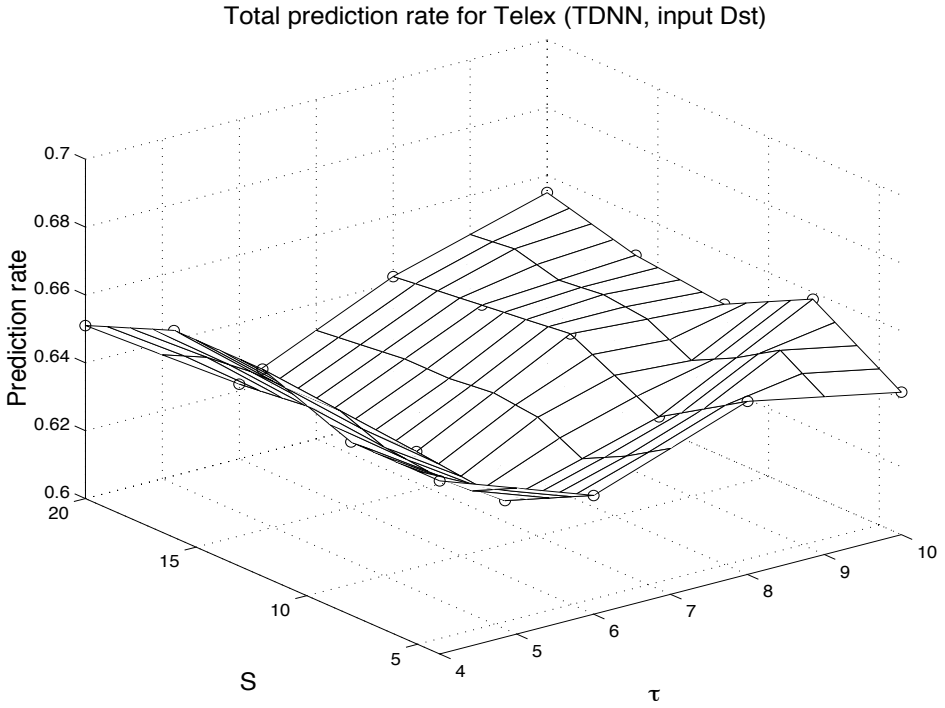
Total prediction rate for Telex (TDNN, input Dst)
Prediction rate
0.7
0.68
0.66
0.64
0.62
0.6
20
15
10
5
S
4
5
6
7
8
9
10
τ

(e)

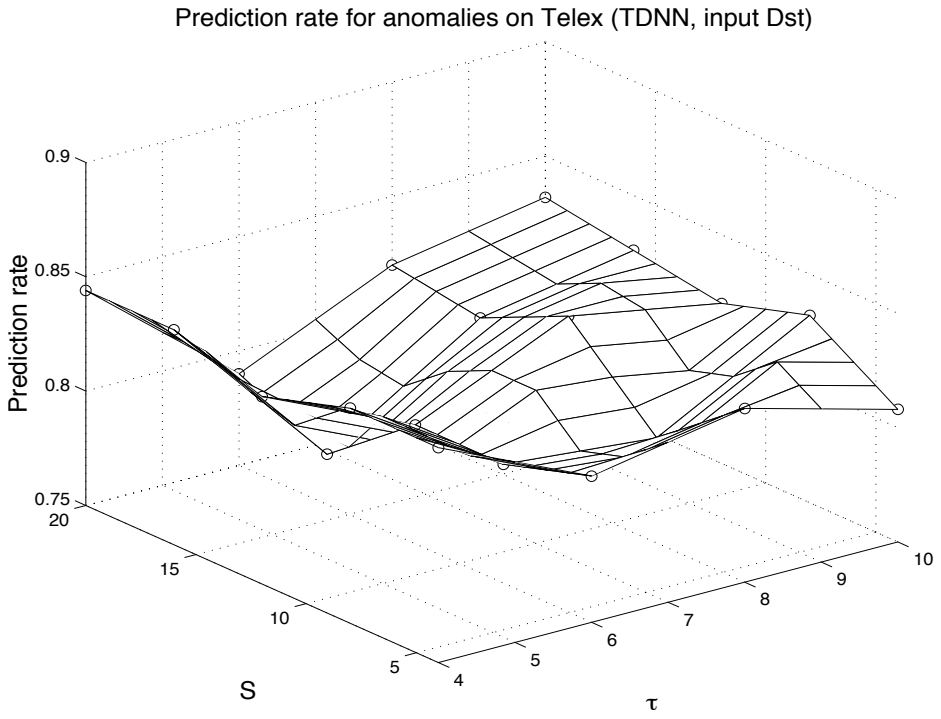
Prediction rate for anomalies on Telex (TDNN, input Dst)
Prediction rate
0.9
0.85
0.8
0.75
20
15
10
5
S
4
5
6
7
8
9
10
τ

(f)

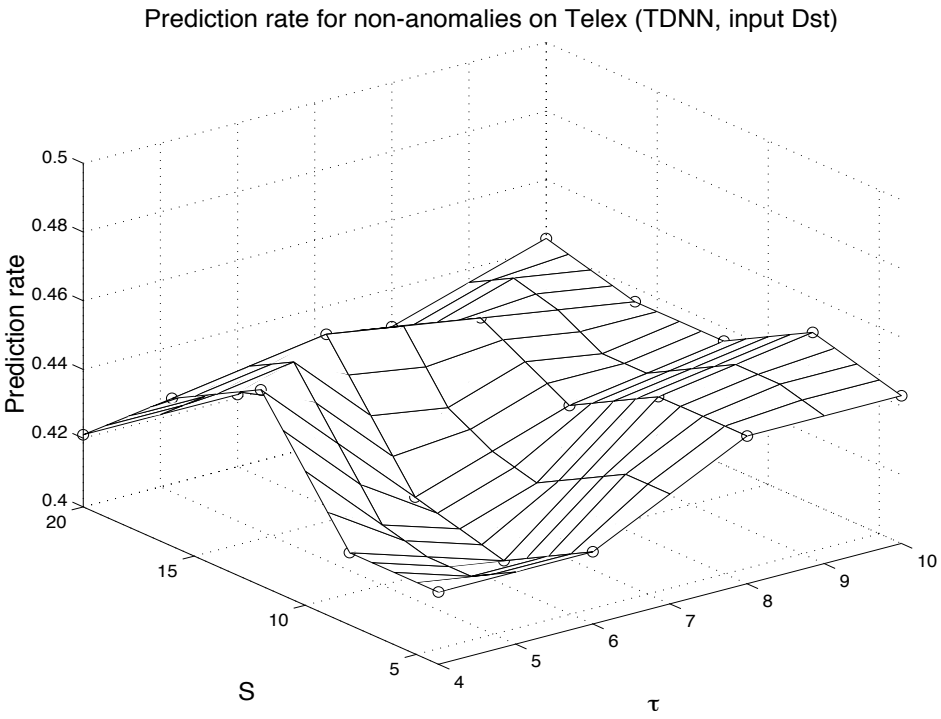
Prediction rate for non-anomalies on Telex (TDNN, input Dst)
Prediction rate
0.5
0.48
0.46
0.44
0.42
0.4
20
15
10
5
S
4
5
6
7
8
9
10
τ

(g)

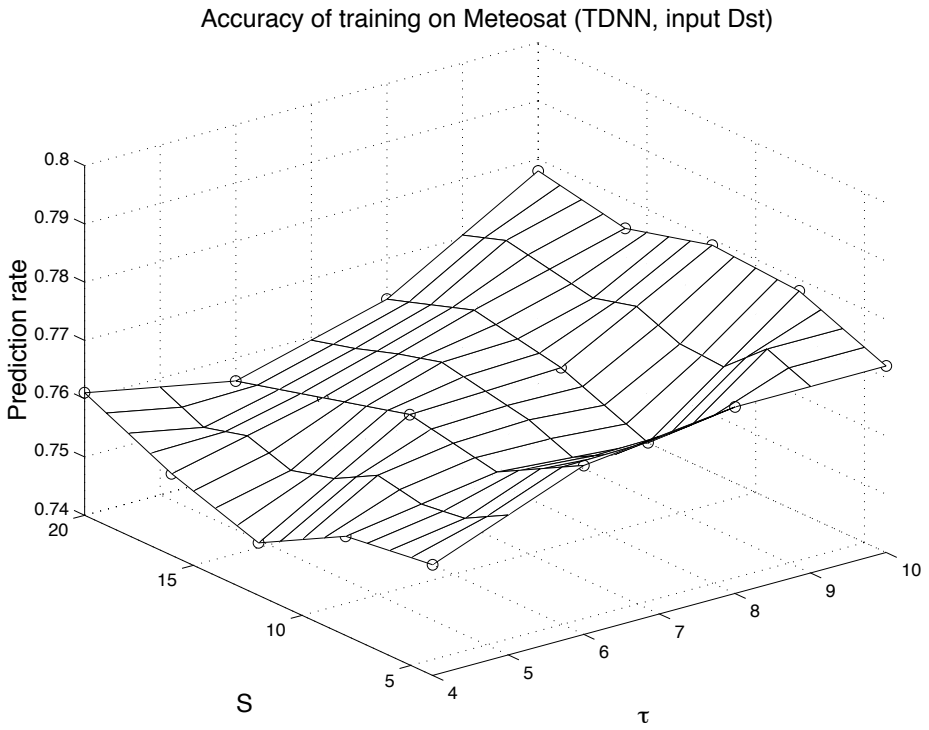
Accuracy of training on Meteosat (TDNN, input Dst)
Prediction rate
0.8
0.79
0.78
0.77
0.76
0.75
0.74
20
15
10
5
S
4
5
6
7
8
9
10
τ

(h)

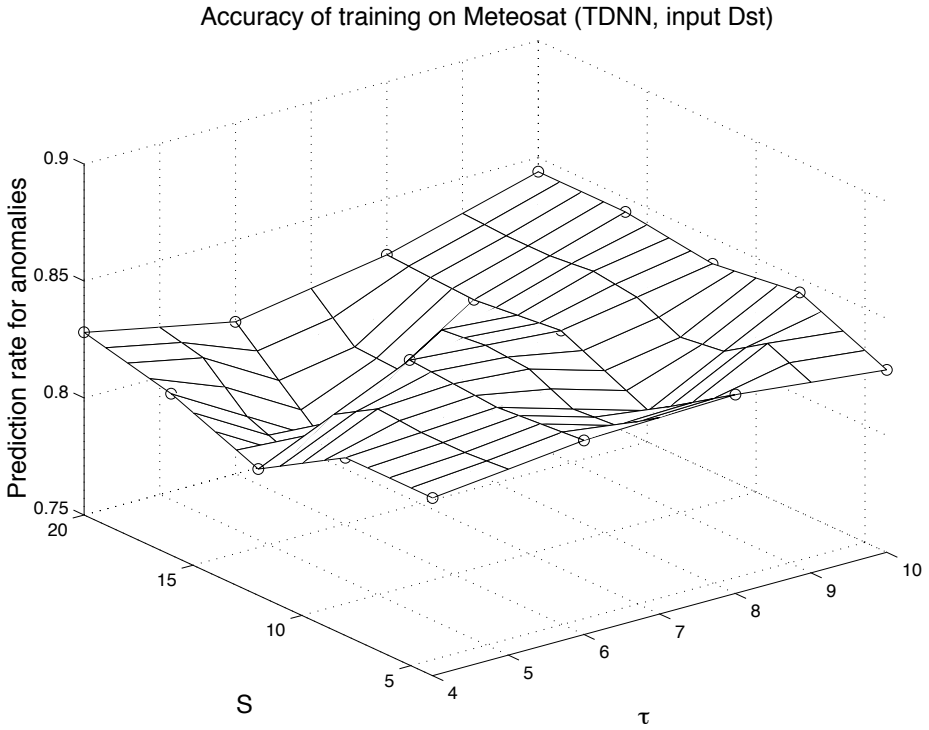
Accuracy of training on Meteosat (TDNN, input Dst)
Prediction rate for anomalies
0.9
0.85
0.8
0.75
20
15
10
5
S
4
5
6
7
8
9
10
τ

(i)

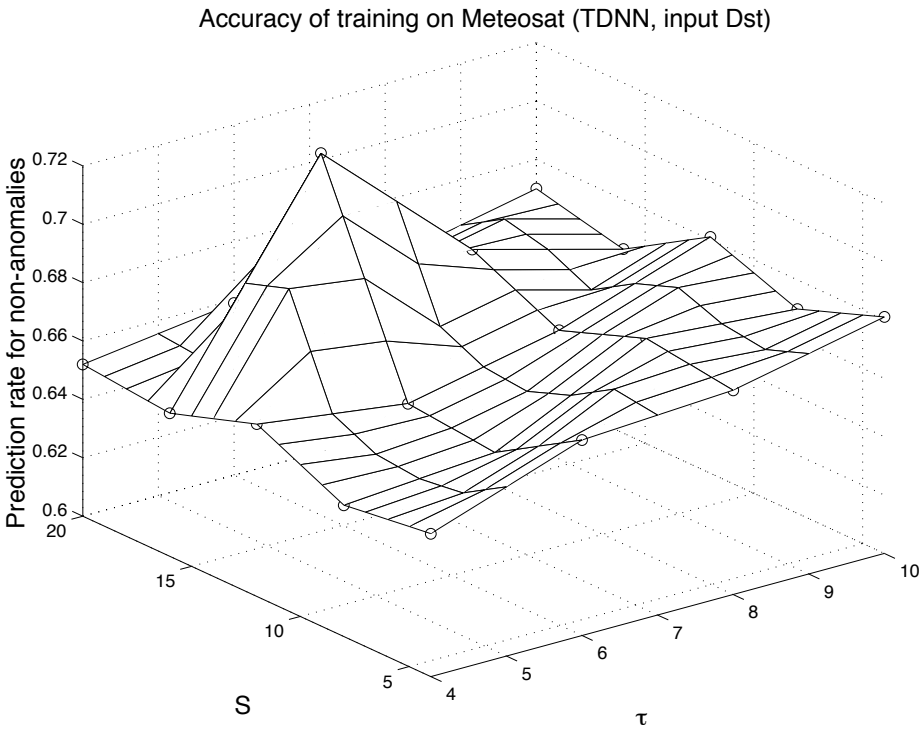

Figure 4. *Predictions one day ahead from the input Dst using TDNN in terms of the network architecture (i.e., the time delay line and the number of hidden neurons). (a) Total prediction rate for Meteosat-3; (b) Prediction rate for anomalies on Meteosat-3; (c) Prediction rate for non-anomalies on Meteosat-3; (d) Total prediction rate for Tele-X; (e) Prediction rate for anomalies on Tele-X; (f) Prediction rate for non-anomalies on Tele-X; (g) Training accuracy on Meteosat-3; (h) Training accuracy for anomalies on Meteosat-3; (i) Training accuracy for non-anomalies on Meteosat-3;*

The total prediction accuracy is rather stable in terms of time delay line and number of hidden neurons with Dst as input. The total prediction rate varies between 69% and 73% for events on Meteosat-3 while the total prediction rate varies between 62% and 66% for Tele-X.

The prediction rate varies between 70% and 80% for anomalies and between 56% and 72% for non-anomalies on Meteosat-3. For Tele-X, the prediction rate varies between 77% and 84% for anomalies and between 41% and 46% for non-anomalies.

4.2.3 Case study 3: Input electron flux (E > 2 MeV)

For the electron flux being the input parameter, we summarise the prediction results in Table 6 and Figures 5(a)-(i) in terms of the time delay line and the number of the network hidden neurons.

Table 6. One day ahead prediction of spacecraft anomalies from eflux (TDNN)

$\tau(days)$	S	R_{te}	R_{te1}	R_{te2}	R_{tlx}	R_{tlx1}	R_{tlx2}	R_{tr}	R_{tr1}	R_{tr2}
4	4	0.587	0.761	0.390	0.648	0.868	0.386	0.675	0.813	0.452
4	8	0.620	0.862	0.348	0.674	0.934	0.364	0.673	0.861	0.366
4	12	0.613	0.836	0.362	0.648	0.886	0.364	0.681	0.850	0.405
4	16	0.593	0.811	0.348	0.648	0.892	0.357	0.674	0.848	0.391
4	20	0.593	0.704	0.468	0.642	0.772	0.486	0.643	0.696	0.556
6	4	0.577	0.736	0.397	0.642	0.868	0.371	0.692	0.830	0.466
6	8	0.587	0.761	0.390	0.622	0.862	0.336	0.679	0.824	0.444
6	12	0.580	0.792	0.340	0.625	0.880	0.321	0.670	0.835	0.401
6	16	0.540	0.623	0.447	0.642	0.826	0.421	0.675	0.760	0.538
6	20	0.540	0.723	0.333	0.651	0.880	0.379	0.682	0.835	0.434
8	4	0.583	0.780	0.362	0.651	0.862	0.400	0.690	0.848	0.434
8	8	0.547	0.635	0.447	0.635	0.796	0.443	0.696	0.778	0.563
8	12	0.573	0.723	0.404	0.629	0.832	0.386	0.696	0.837	0.466
8	16	0.563	0.673	0.440	0.635	0.826	0.407	0.707	0.835	0.498
8	20	0.573	0.717	0.411	0.619	0.826	0.371	0.709	0.846	0.487
10	4	0.560	0.667	0.440	0.651	0.820	0.450	0.704	0.815	0.523
10	8	0.563	0.679	0.433	0.629	0.832	0.386	0.697	0.846	0.455
10	12	0.553	0.610	0.489	0.629	0.820	0.400	0.737	0.833	0.581
10	16	0.520	0.629	0.397	0.609	0.802	0.379	0.722	0.837	0.534
10	20	0.550	0.572	0.525	0.609	0.743	0.450	0.744	0.822	0.616

(a)

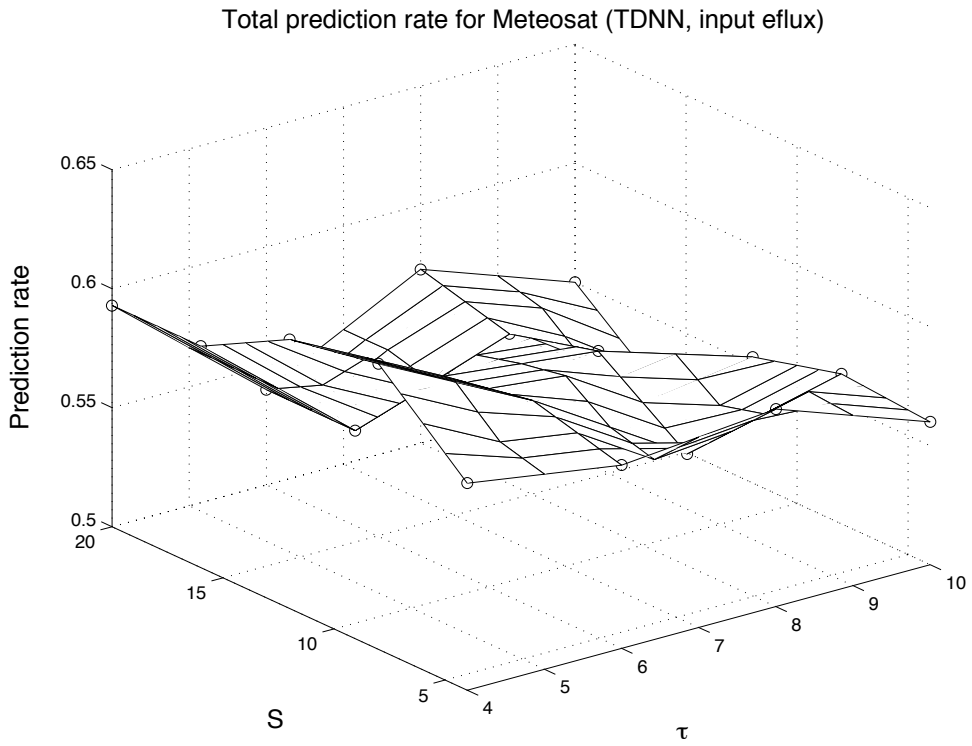
Total prediction rate for Meteosat (TDNN, input eflux)
Prediction rate
0.65
0.6
0.55
0.5
20
15
10
5
S
4
5
6
7
8
9
10
τ

(b)

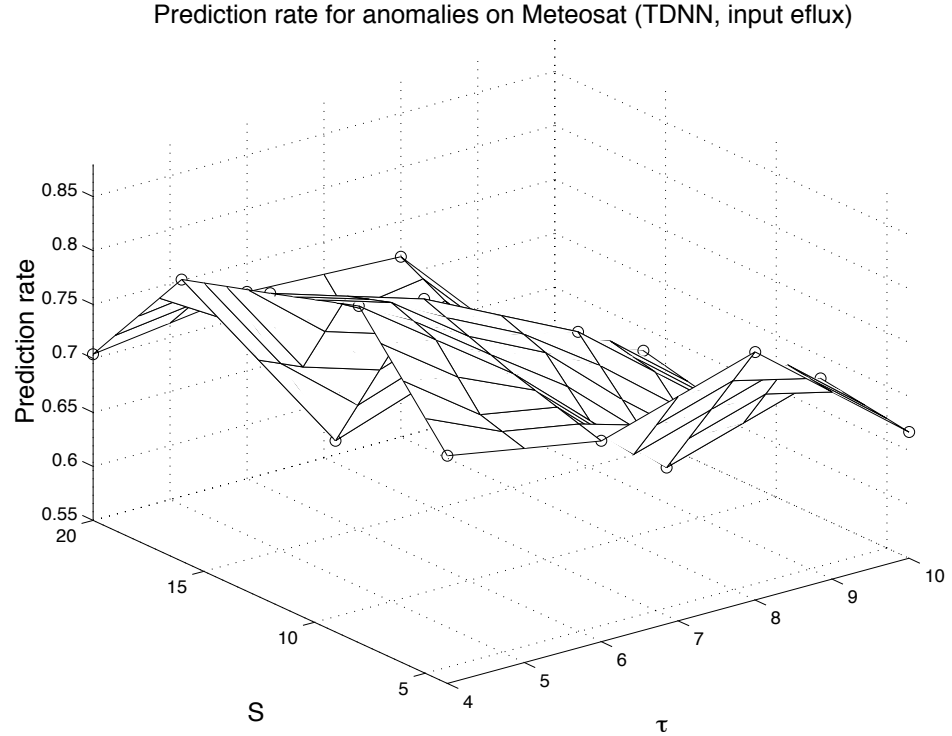
Prediction rate for anomalies on Meteosat (TDNN, input eflux)
Prediction rate
0.85
0.8
0.75
0.7
0.65
0.6
0.55
20
15
10
5
S
4
5
6
7
8
9
10
τ

(c)

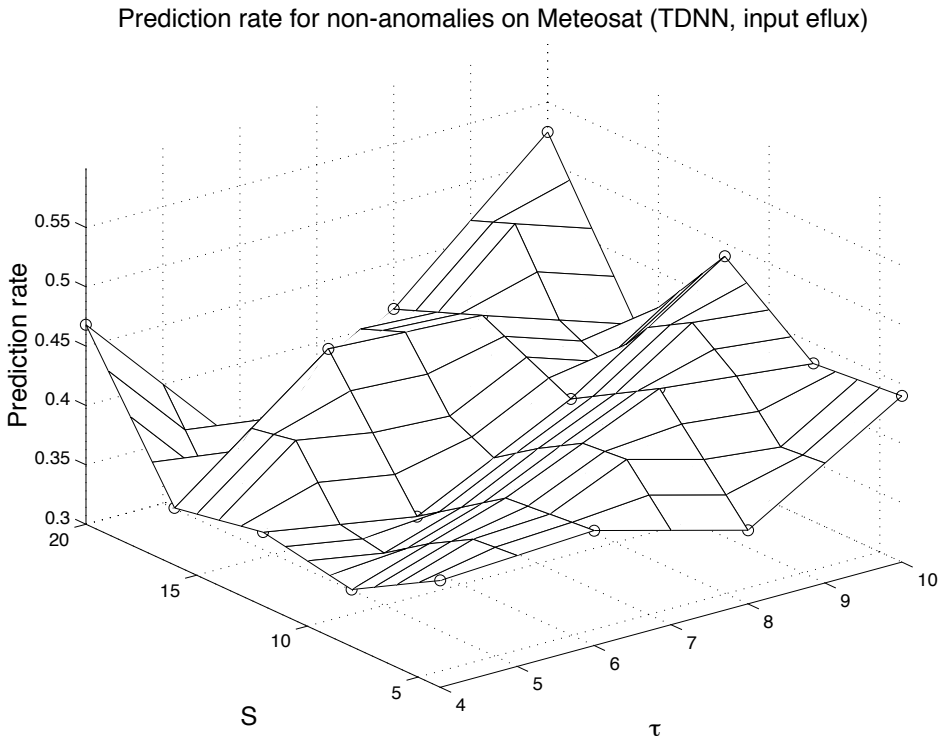
Prediction rate for non-anomalies on Meteosat (TDNN, input eflux)
Prediction rate
0.55
0.5
0.45
0.4
0.35
0.3
20
15
10
5
S
4
5
6
7
8
9
10
τ

(d)

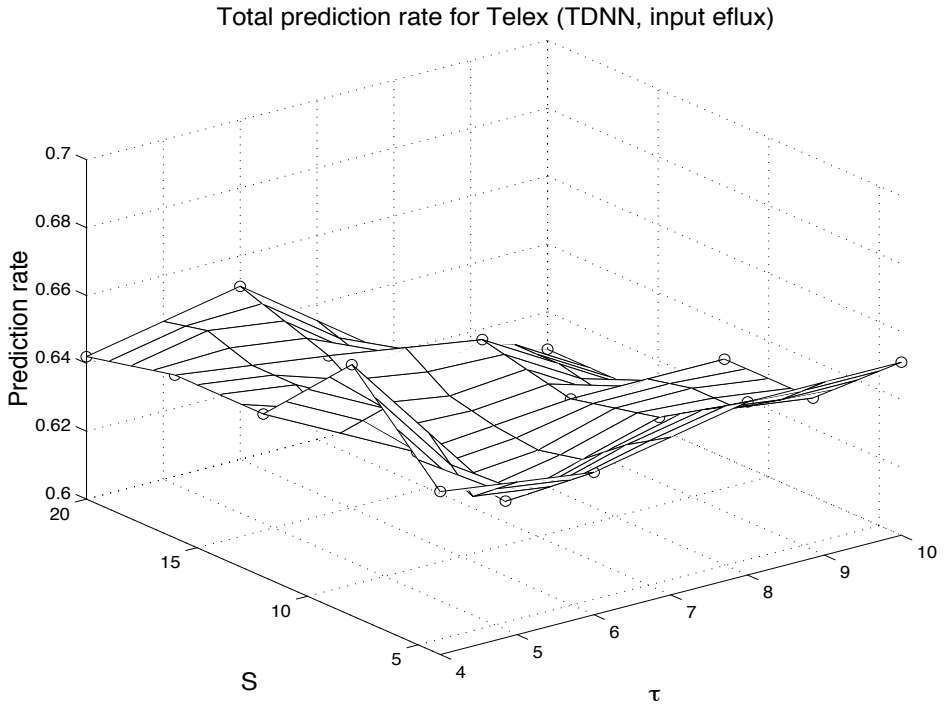
Total prediction rate for Telex (TDNN, input eflux)
Prediction rate
0.7
0.68
0.66
0.64
0.62
0.6
20
15
10
5
S
4
5
6
7
8
9
10
τ

(e)

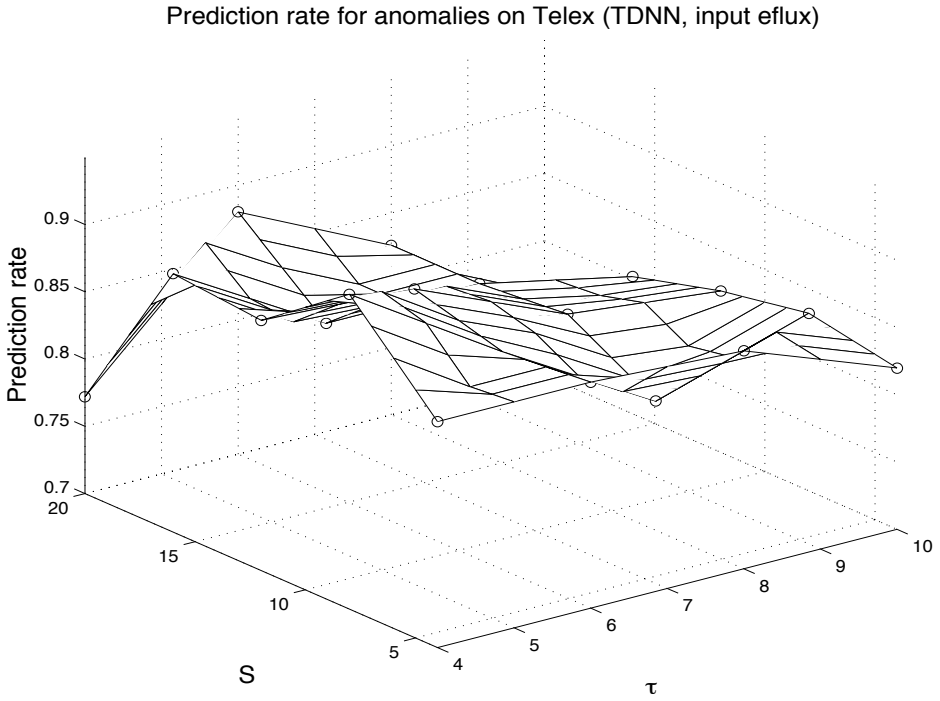
Prediction rate for anomalies on Telex (TDNN, input eflux)
Prediction rate
0.9
0.85
0.8
0.75
0.7
20
15
10
5
S
4
5
6
7
8
9
10
τ

(f)

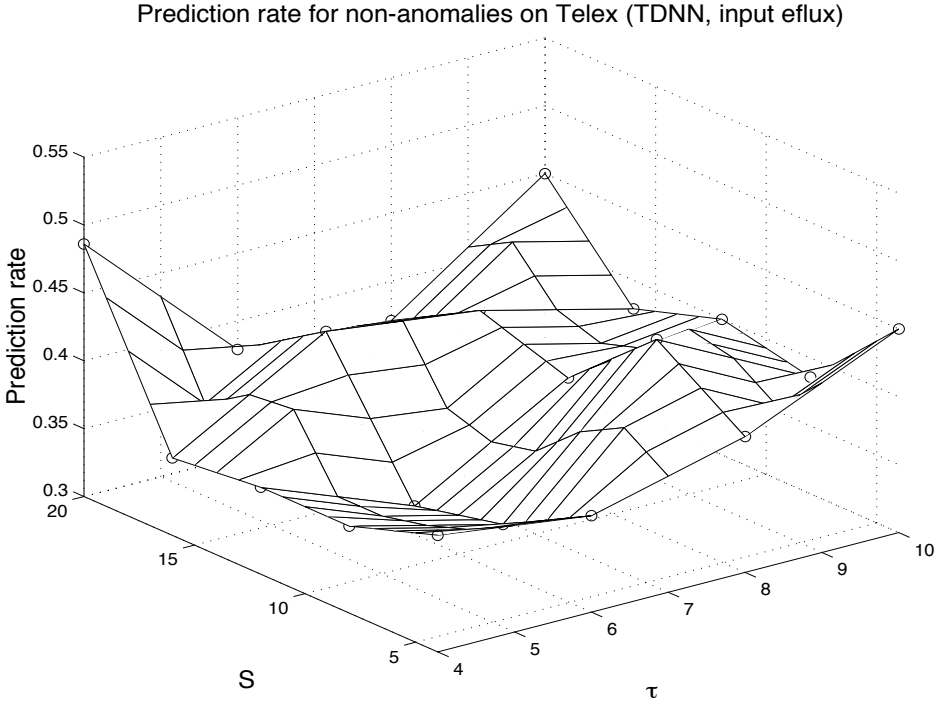
Prediction rate for non-anomalies on Telex (TDNN, input eflux)
Prediction rate
0.55
0.5
0.45
0.4
0.35
0.3
20
15
10
5
S
4
5
6
7
8
9
10
τ

(g)

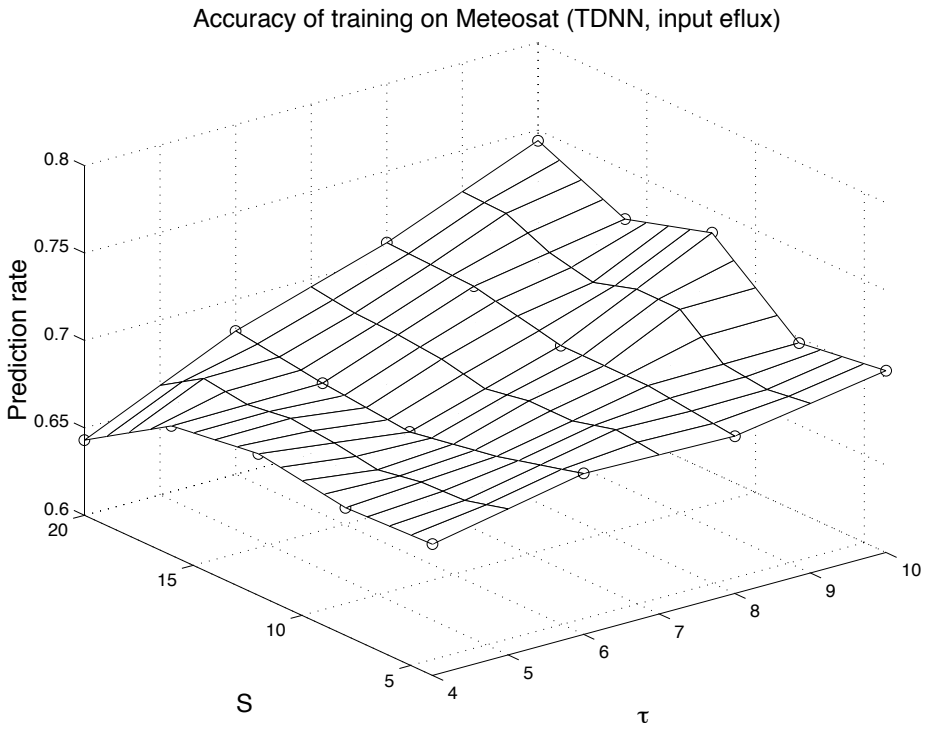
Accuracy of training on Meteosat (TDNN, input eflux)
Prediction rate
0.8
0.75
0.7
0.65
0.6
20
15
10
5
S
4
5
6
7
8
9
10
τ

(h)

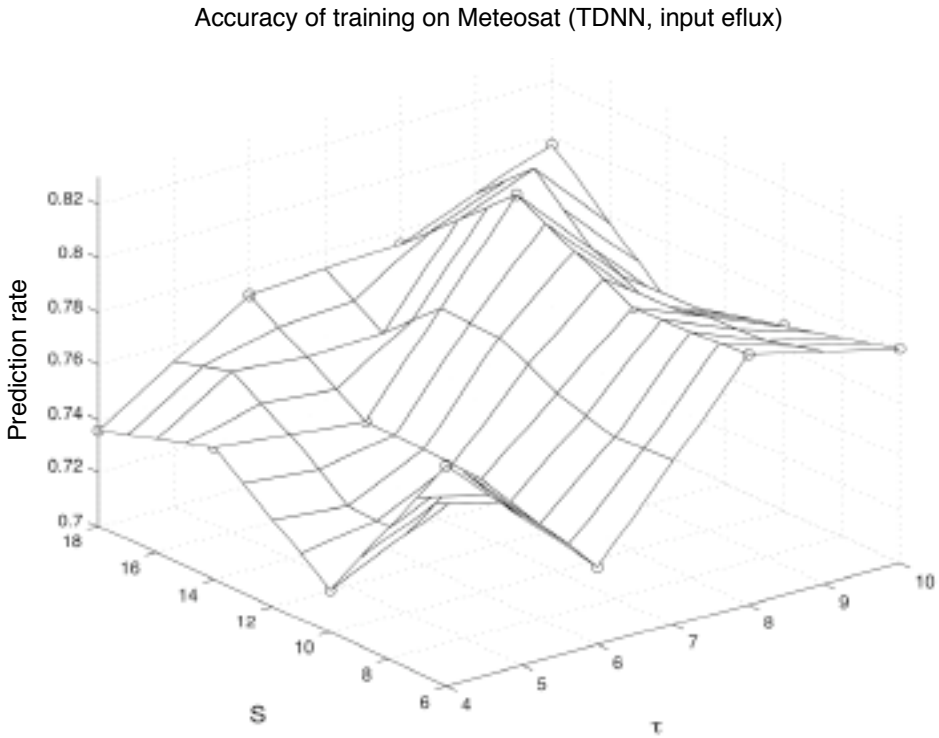
Accuracy of training on Meteosat (TDNN, input eflux)
Prediction rate
0.82
0.8
0.78
0.76
0.74
0.72
0.7
18
16
14
12
10
8
6
S
4
5
6
7
8
9
10
τ

(i)

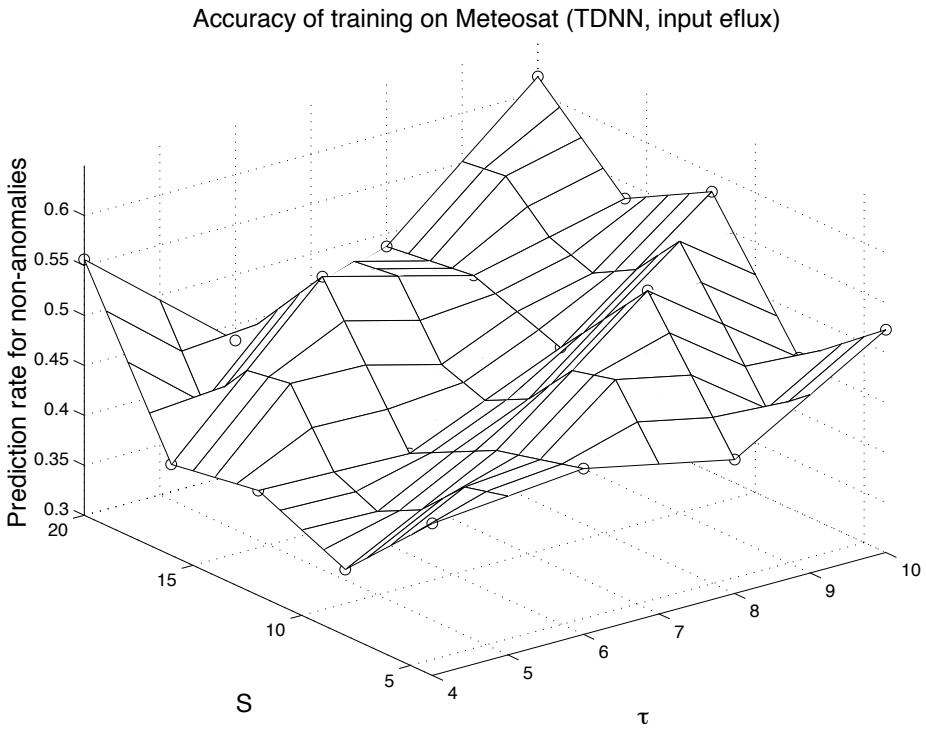

Figure 5. *Predictions one day ahead from the input energetic electron flux (E > 2 MeV) using TDNN in terms of the network architecture (i.e., the time delay line and the number of hidden neurons). (a) Total prediction rate for Meteosat-3; (b) Prediction rate for anomalies on Meteosat-3; (c) Prediction rate for non-anomalies on Meteosat-3; (d) Total prediction rate for Tele-X; (e) Prediction rate for anomalies on Tele-X; (f) Prediction rate for non-anomalies on Tele-X; (g) Training accuracy on Meteosat-3; (h) Training accuracy for anomalies on Meteosat-3; (i) Training accuracy for non-anomalies on Meteosat-3;*

As can be seen from Table 6, the total prediction rate varies between 52% and 62% for the events (included in the validation set) on Meteosat-3, the prediction rate is in the range 57-86 percent for anomalies on Meteosat-3 and in the range 33-53 percent for non-anomalies on Meteosat-3. For Tele-X, the total prediction rate ranges from 61% to 67%, the prediction rate ranges from 74% to 93% for anomalies and from 32% to 49% for non-anomalies.

The energetic electron flux allows to predict anomalies much more accurately than to predict non-anomalies. It might well imply that if energetic electron flux is high, then anomalies will probably occur and that if energetic electron flux is low, it is still possible to have anomalies which are caused by some other factors, e.g., lower-energy electron flux. When we look at the training error, it can be found that training accuracy (above 80%) for anomalies is much higher than that (37% to 62%) for non-anomalies. We can see from the training that the

energetic electron flux is not allowing to well predict non-anomalies. Adding more than one spacecraft to define times without anomalies should, however, give better information on when the environment conditions are likely not to give rise to anomalies.

In contrast, when the input is Kp or Dst, during training the training accuracy for non-anomalies ranges between 61% and 70% for the input Kp and ranges between 64% and 72% for the input Dst.

The best model for different number of the network hidden neurons versus the length of the time delay line is further summarized in Figure 6.

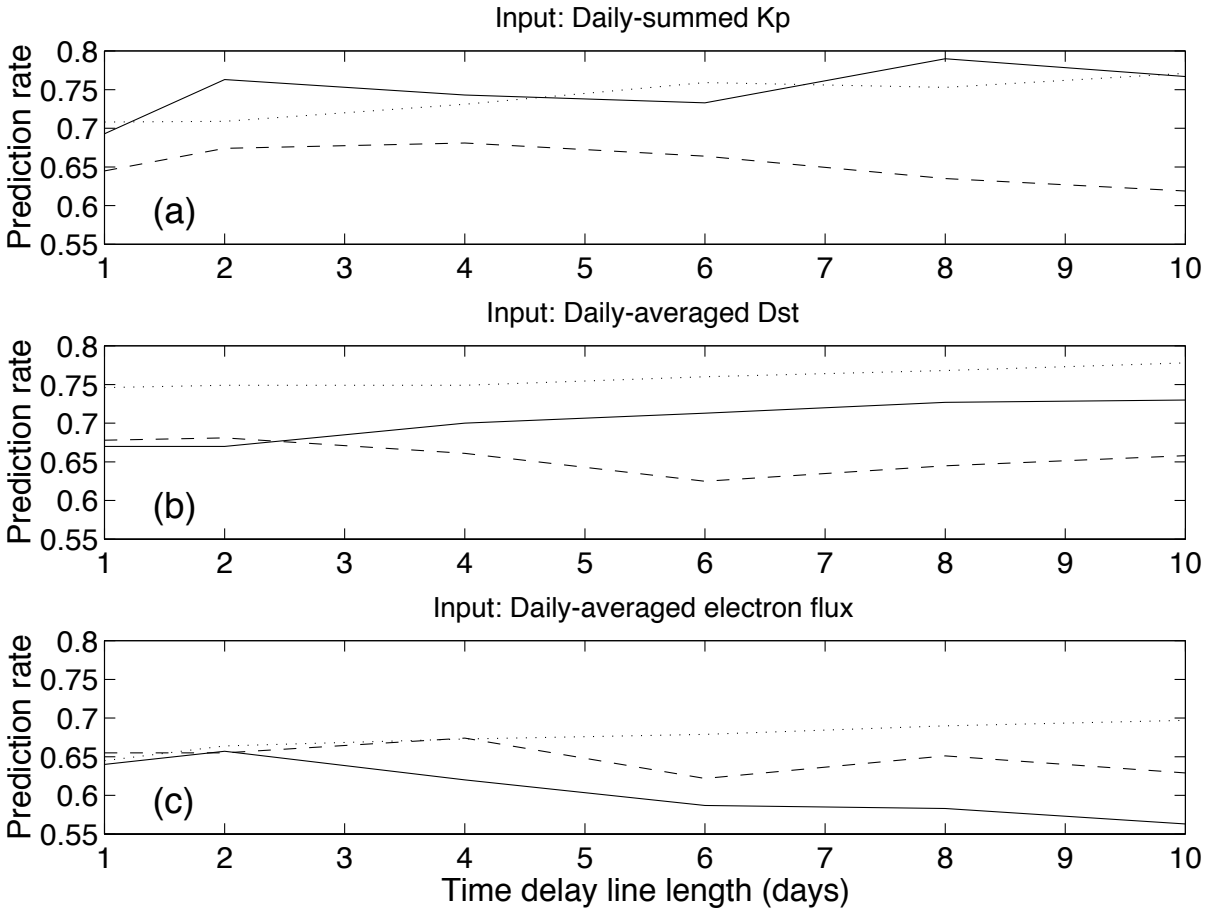

Figure 6. *The total prediction rate for both anomalies and non-anomalies versus the length of the time delay line in the network input layer, with the input parameter: (a) Daily-summed Kp; (b) Daily-averaged Dst (nT); and (c) Daily-averaged energetic electron flux with energy above 2 MeV ($cm^{-2}s^{-1}sr^{-1}$). The solid line stands for the total prediction rate on Meteosat-3, the dashed line for the total prediction rate on Tele-X, and the dotted line for the prediction rate for training on the events on Meteosat-3.*

4.2.4 Case study 4: Combined inputs

We have used the combined inputs in order to get a better prediction results. However, we found that the accuracy does not improve. The main reason is that the input parameters; electron flux, Dst and Kp are statistically inter-correlated, as shown in [Koons and Gorney, 1991]. So the input dimension does not increase in essence.

4.3 Predictions using learning vector quantization network

We have used two network paradigms (TDNN and LVQN) and found that they give similar prediction accuracy. For a comparison, we present the results with Kp and energetic electron flux as input, respectively. For the input Kp, we carry out a more detailed study as we did using TDNN.

4.3.1 Case study 1: Input Kp

The prediction results are given in Table 7 and Figures 7(a)-(i). Comparing Table 4 and Table 7 we see that the two network paradigms give similar accuracy.

Table 7. One day ahead prediction of spacecraft anomalies from Kp (LVQN)

τ(days)	S	η_{te}	η_{te1}	η_{te2}	η_{tlx}	η_{tlx1}	η_{tlx2}	η_{tr}	η_{tr1}	η_{tr2}
4	6	0.730	0.805	0.645	0.671	0.814	0.500	0.722	0.782	0.624
4	10	0.717	0.723	0.709	0.658	0.707	0.600	0.697	0.716	0.667
4	14	0.733	0.742	0.723	0.664	0.766	0.543	0.726	0.749	0.688
4	18	0.740	0.736	0.745	0.687	0.772	0.586	0.727	0.736	0.713
6	6	0.710	0.723	0.695	0.655	0.778	0.507	0.689	0.729	0.624
6	10	0.727	0.723	0.730	0.648	0.725	0.557	0.724	0.742	0.695
6	14	0.743	0.736	0.752	0.674	0.784	0.543	0.718	0.744	0.674
6	18	0.740	0.730	0.752	0.661	0.784	0.514	0.738	0.771	0.685
8	6	0.767	0.755	0.780	0.638	0.796	0.450	0.746	0.793	0.670
8	10	0.790	0.761	0.823	0.635	0.778	0.464	0.739	0.791	0.656
8	14	0.807	0.792	0.823	0.645	0.820	0.436	0.759	0.813	0.670
8	18	0.797	0.748	0.851	0.671	0.772	0.550	0.741	0.775	0.685
10	6	0.777	0.736	0.823	0.612	0.766	0.429	0.718	0.780	0.616
10	10	0.763	0.667	0.872	0.645	0.743	0.529	0.741	0.769	0.695
10	14	0.777	0.698	0.865	0.642	0.731	0.536	0.737	0.758	0.703
10	18	0.813	0.742	0.894	0.655	0.737	0.557	0.763	0.797	0.706

(a)

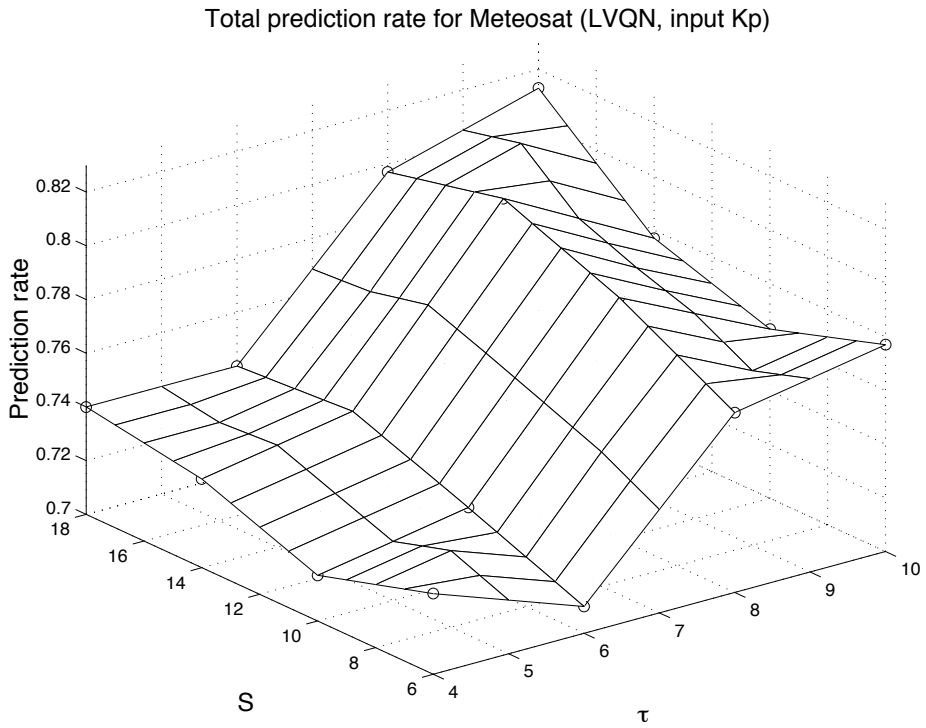
Total prediction rate for Meteosat (LVQN, input Kp)
Prediction rate
0.82
0.8
0.78
0.76
0.74
0.72
0.7
18
16
14
12
10
8
6
S
4
5
6
7
8
9
10
τ

(b)

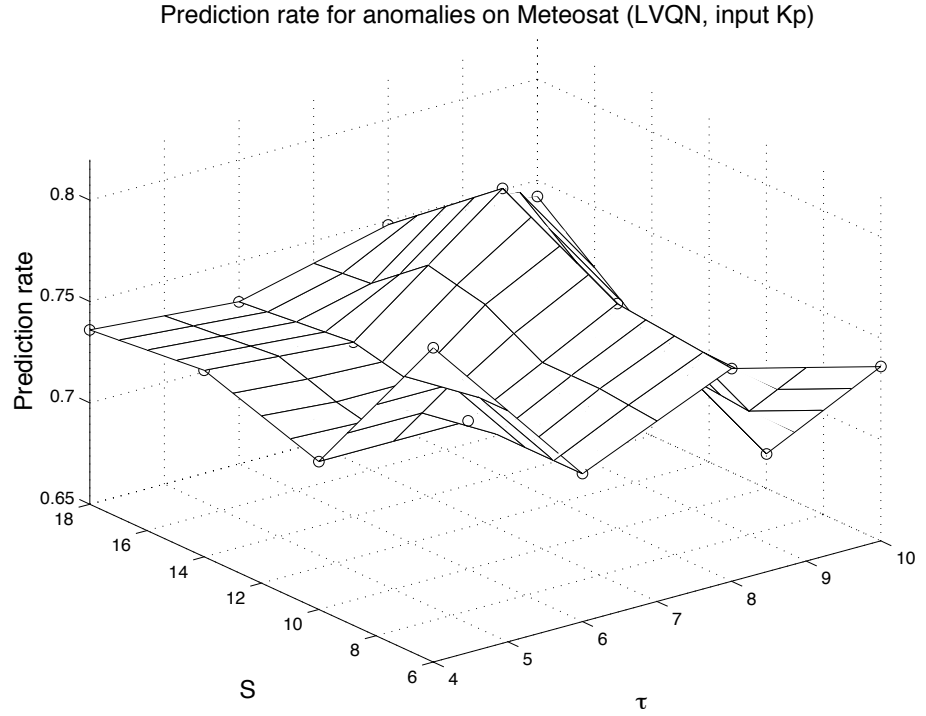
Prediction rate for anomalies on Meteosat (LVQN, input Kp)
Prediction rate
0.8
0.75
0.7
0.65
18
16
14
12
10
8
6
S
4
5
6
7
8
9
10
τ

(c)

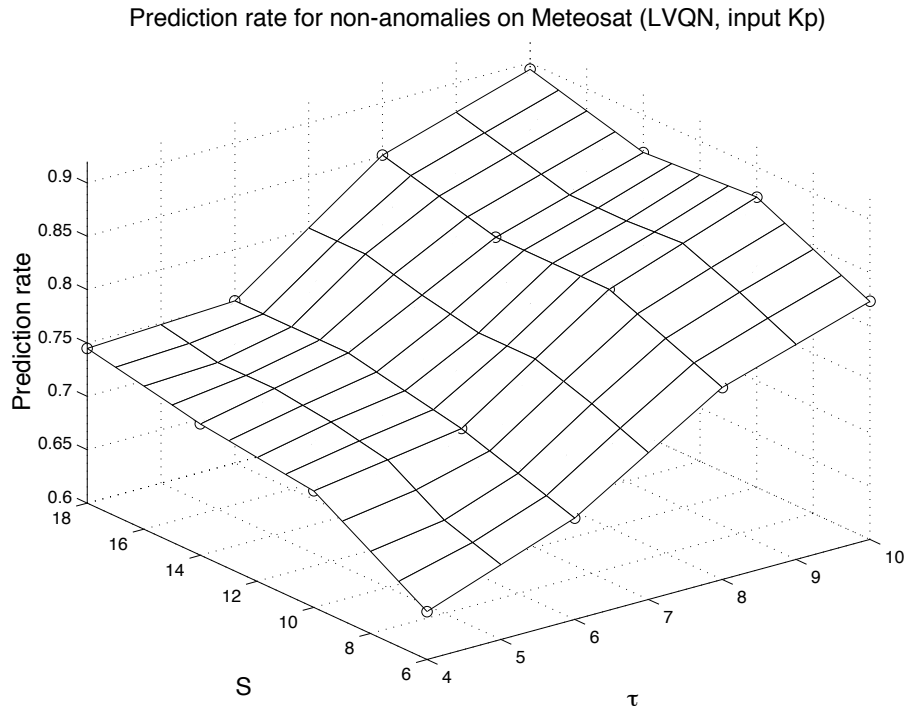
Prediction rate for non-anomalies on Meteosat (LVQN, input Kp)
Prediction rate
0.9
0.85
0.8
0.75
0.7
0.65
0.6
18
16
14
12
10
8
6
S
4
5
6
7
8
9
10
τ

(d)

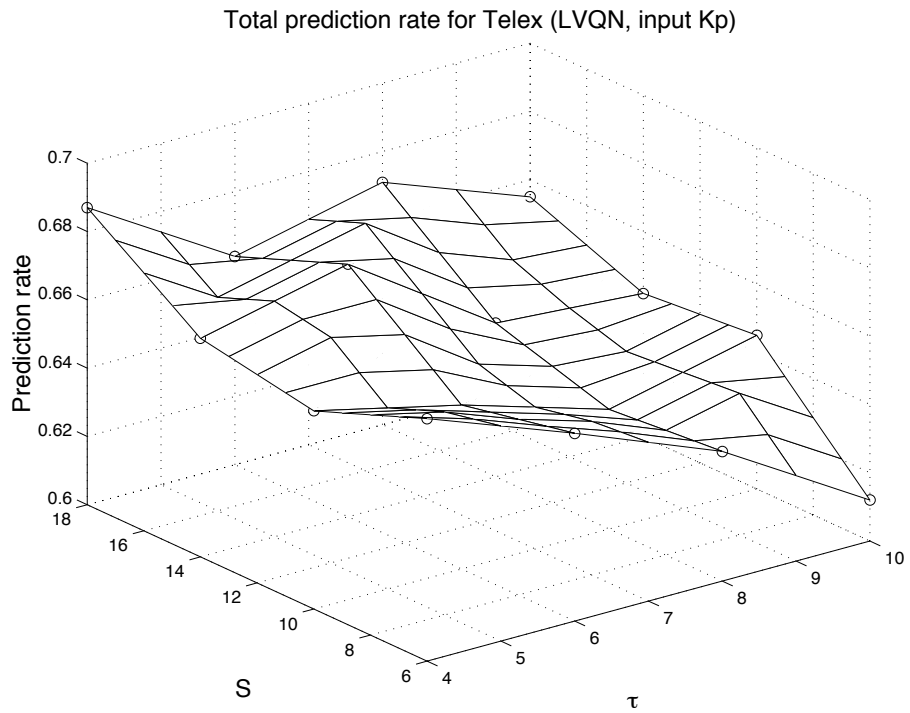
Total prediction rate for Telex (LVQN, input Kp)
Prediction rate
0.7
0.68
0.66
0.64
0.62
0.6
18
16
14
12
10
8
6
S
4
5
6
7
8
9
10
τ

(e)

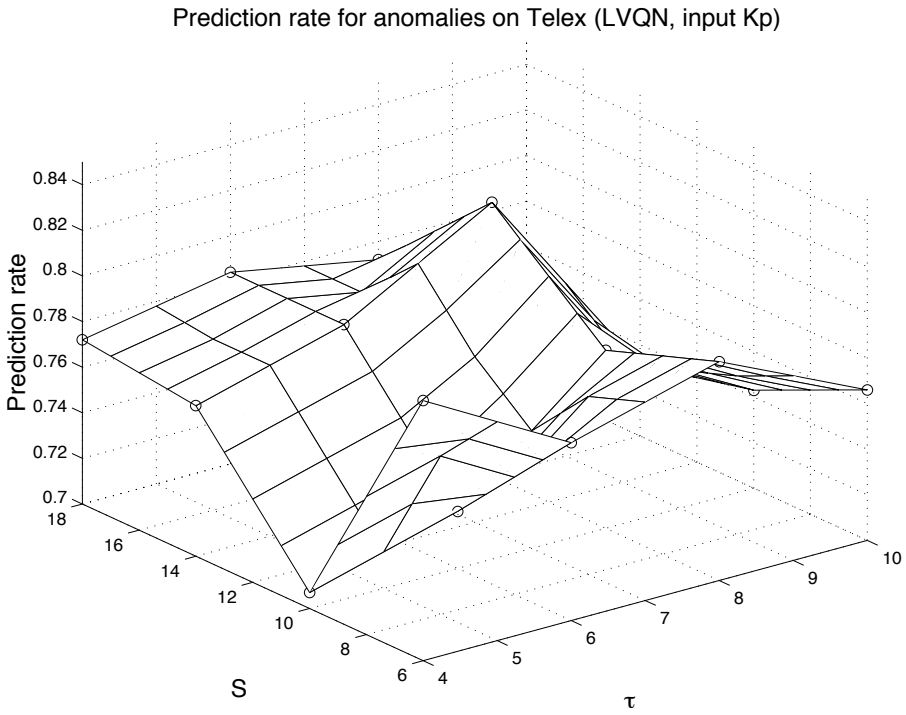
Prediction rate for anomalies on Telex (LVQN, input Kp)
Prediction rate
0.84
0.82
0.8
0.78
0.76
0.74
0.72
0.7
18
16
14
12
10
8
6
S
4
5
6
7
8
9
10
τ

(f)

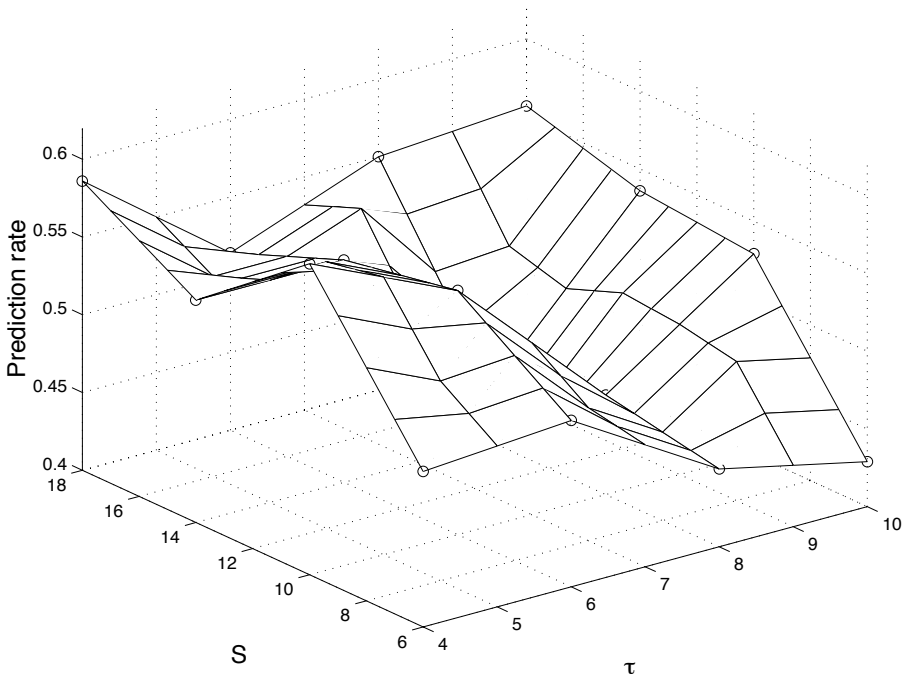
Prediction rate for non-anomalies on Telex (LVQN, input Kp)
Prediction rate
0.6
0.55
0.5
0.45
0.4
18
16
14
12
10
8
6
S
4
5
6
7
8
9
10
τ

(g)

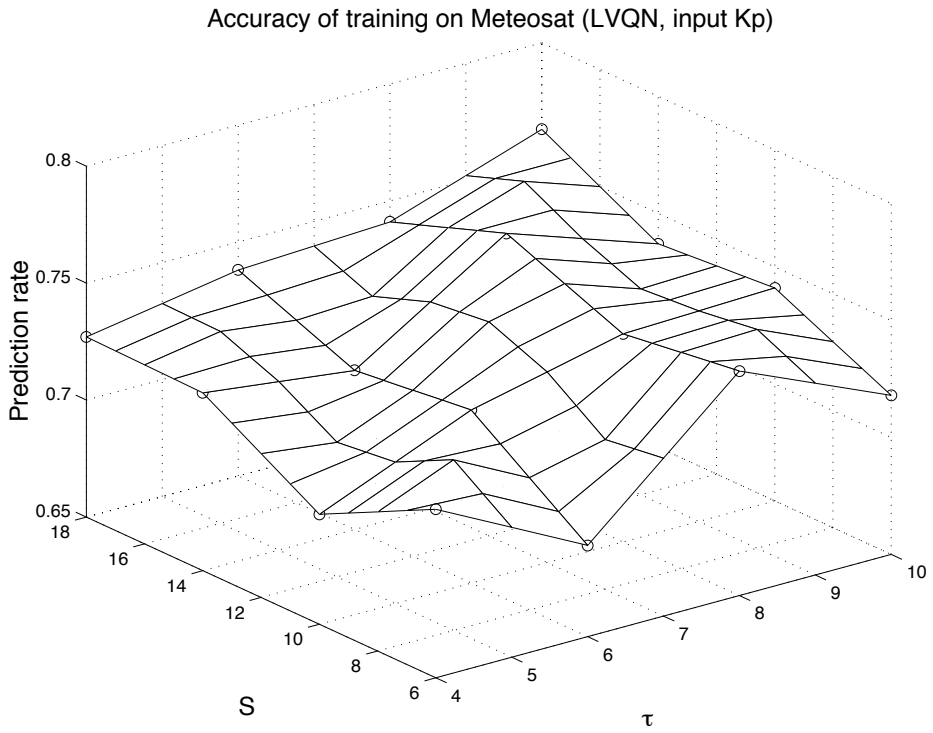
Accuracy of training on Meteosat (LVQN, input Kp)
Prediction rate
0.8
0.75
0.7
0.65
18
16
14
12
10
8
6
S
4
5
6
7
8
9
10
τ

(h)

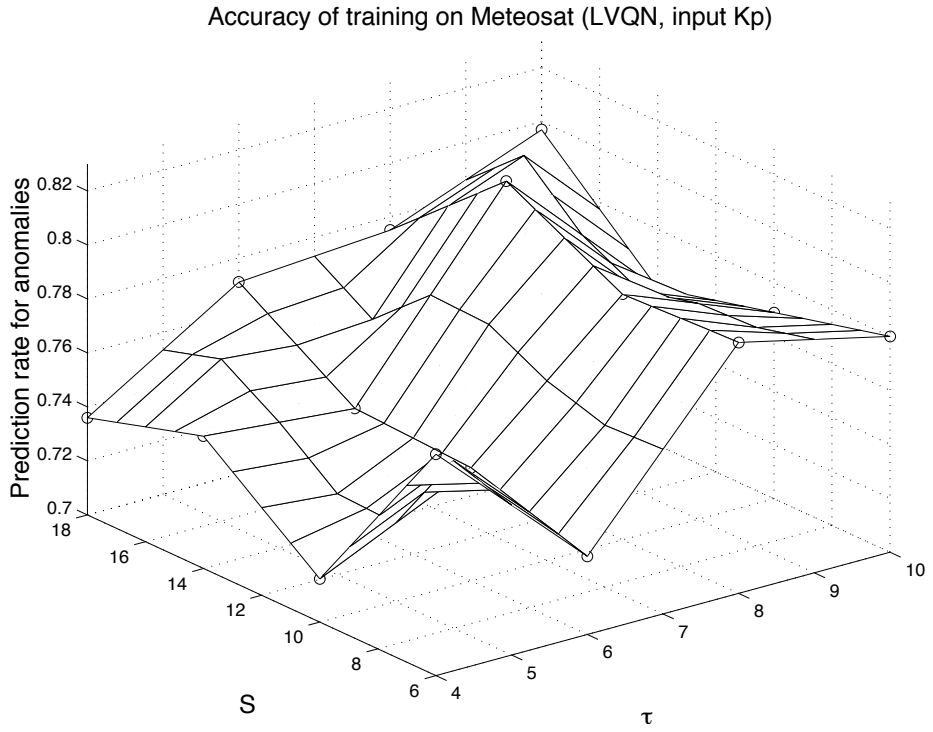
Accuracy of training on Meteosat (LVQN, input Kp)
Prediction rate for anomalies
0.82
0.8
0.78
0.76
0.74
0.72
0.7
18
16
14
12
10
8
6
S
4
5
6
7
8
9
10
τ

(i)

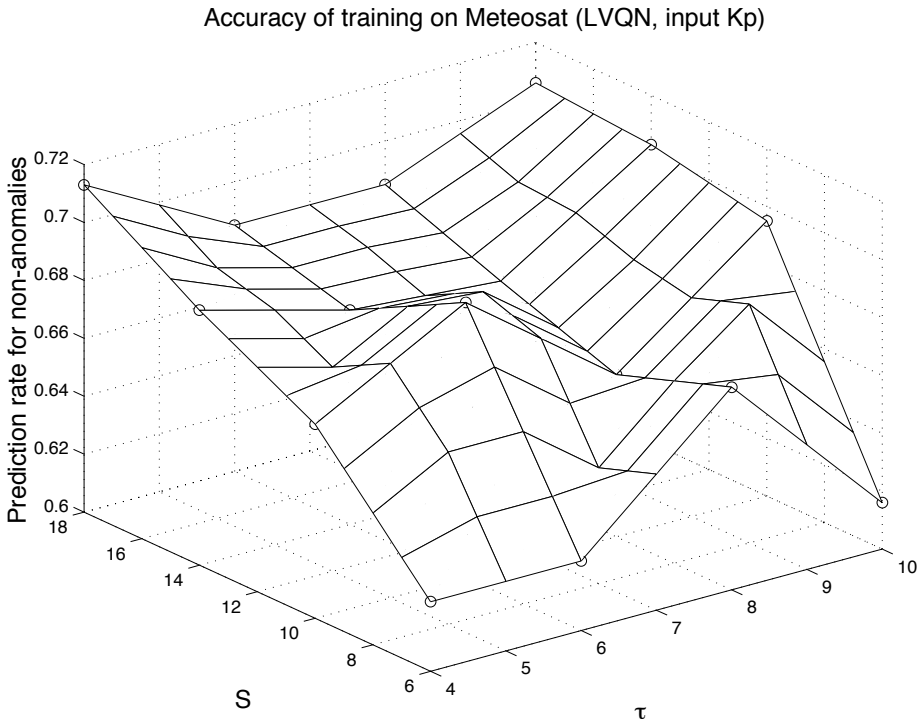

Figure 7. *Predictions one day ahead from the input Kp using LVQN in terms of the network architecture (i.e., the time delay line and the number of hidden neurons). (a) Total prediction rate for Meteosat-3; (b) Prediction rate for anomalies on Meteosat-3; (c) Prediction rate for non-anomalies on Meteosat-3; (d) Total prediction rate for Tele-X; (e) Prediction rate for anomalies on Tele-X; (f) Prediction rate for non-anomalies on Tele-X; (g) Training accuracy on Meteosat-3; (h) Training accuracy for anomalies on Meteosat-3; (i) Training accuracy for non-anomalies on Meteosat-3;*

4.3.2 Case study 2: Input electron flux (E > 2 MeV)

With electron flux as the input, the results are given in Table 8. The accuracy is slightly lower than that using TDNN.

Table 8. One day ahead prediction of spacecraft anomalies from eflux (LVQN)

$\tau(days)$	S	R_{te}	R_{te1}	R_{te2}	R_{tlx}	R_{tlx1}	R_{tlx2}	R_{tr}	R_{tr1}	R_{tr2}
6	6	0.543	0.654	0.418	0.645	0.760	0.507	0.614	0.696	0.480
6	10	0.513	0.604	0.411	0.704	0.778	0.614	0.628	0.685	0.534
6	14	0.557	0.629	0.475	0.678	0.772	0.564	0.628	0.705	0.502
6	18	0.527	0.572	0.475	0.671	0.760	0.564	0.656	0.731	0.534
8	6	0.583	0.792	0.348	0.648	0.832	0.429	0.622	0.747	0.419
8	10	0.537	0.597	0.468	0.687	0.754	0.607	0.608	0.630	0.573
8	14	0.527	0.623	0.418	0.674	0.784	0.543	0.632	0.707	0.509
8	18	0.550	0.572	0.525	0.681	0.760	0.586	0.640	0.676	0.581

5 Discussion

For Meteosat-3, Kp gives slightly better predictions than Dst, whereas relativistic electron flux gives prediction rates some 10% less than Kp and Dst. This is in agreement with the results from the above superposed epoch analysis. As described in Section 2.4, Kp includes contributions from both the substorm currents and the ring current, thereby giving a fairly global characterisation of the energy input into the magnetosphere [Menvielle and Berthelier, 1991]. Dst has contributions mainly from the equatorial ring current, serving as an indicator of the storm intensity. Since Kp is a more global measure of geomagnetic activity than Dst, including contributions from both substorms and storms, it may in general provide better predictions than Dst.

During increasing geomagnetic activity, electron fluxes with low and high energy are enhanced and may lead to spacecraft surface charging and internal dielectric charging, respectively. As inferred from the above analysis Kp and Dst provide better prediction than the relativistic electron flux (only responsible for internal charging). Because ring current ions and electrons are in the energy range 10-300 keV and energy of injected electrons by substorms are of keV order, more accurate prediction from Kp and Dst may indicate that most of the anomalies on Meteosat-3 were caused by electrons in energy range from several keV up to 300 keV. This energy range can lead to both surface charging and internal charging both could have caused the anomalies on Meteosat-3. We found that energetic electron flux gave slightly higher prediction rate for Tele-X than for Meteosat-3 and that the prediction rates from Kp and Dst were higher for Meteosat than for Tele-X. In addition, the energetic electron flux, Kp, and Dst produce almost the same prediction rate for Tele-X. All these observations confirm the results of the superposed analysis in Section 3.

However, while making such analysis we should be aware that the following factors: occurence of anomaly and non-anomaly is satellite-dependent. The training was performed using Meteosat-3 anomaly only. Nevertheless resulting trained neural networks could be satisfactorily used for predicting Tele-X anomaly with a high level of significance.

As seen from the generalisation performance shown in Figure 6, for Meteosat-3 the prediction rate is relatively stable from the input Kp or Dst as τ=4 Given by the energetic electron flux the prediction rate decreases as τ>2 For Tele-X the prediction rate peaks at τ=4 for the input of Kp and of the energetic electron flux, while τ=2 gives the best prediction rate from the input Dst. This suggests that a time scale for the build up of the conditions leading to anomalies on the two satellites is in the range 2-4 days. This is in agreement with a study by Hilgers et al., [1998].

The developed NN models here can be used to forecast times with higher risks for anomalies in real-time from ACE solar wind data because the NN models which can accurately predict Dst from solar wind data have been available [Wu and Lundstedt, 1996, 1997a, 1997b; Wu et al., 1998]. Also, real-time estimate of Kp can make developed NN models operate in real-time (http://www.sel.noaa.gov/planetary_k.html).

To better describe how satellite anomalies are related to electron flux, we will need electron flux data with energy from low (the order of keV) to high (the order of MeV). This will be able to give a better prediction accuracy.

Combining non-local data with local data as input may reduce error caused by different local conditions and local environments. This is investigated in another technical note (Andersson et al., 1999).

The training was on Meteosat with the threshold of 0.5. For the results given in Tables 4-6, the threshold for an output (of TDNN) to be an anomaly or a non-anomaly is 0.5. The specific criterion is that, if the value of the TDNN output is in the range (0.5 1.5), then the output gives an anomaly prediction and if the value of the TDNN output is in the range (-0.5 0.5) then the output gives a non-anomaly prediction. We can expect that neural network models will not generalise well from one satellite to another due to differences of susceptibility to the environment. To improve the generalisation from one satellite (Meteosat) to another (Tele-X), we try to modify the threshold value for a network output that determine if the output is an anomaly or a non-anomaly for Tele-X. We investigate whether or not the threshold value is satellite-dependent. In other words, we examine if such a threshold value exists that prediction accuracy for anomalies and for non-anomalies is very close to each other as the case for Meteosat with the threshold of 0.5. Nonetheless, it should be noted that the total prediction rate will be unchanged.

For predictions on Tele-X, as we can see from Tables 4-8, the prediction accuracy for non-anomalies is much lower than for anomalies. Therefore we vary the value of the threshold for 2 neural network models (for input Kp and 8 days time window) respectively with 8 and 16 hidden neurons. We obtain the prediction results for Telex in Table 9 and Figure 8. As seen from Figure 8, we have found a new threshold value, which can give better accuracy of non-anomalies at the expense of accuracy for anomalies. This threshold value is 0.63, giving prediction rate of about 65 percent for both anomalies and non-anomalies. The two different models give almost the same value of threshold. Anomaly or non-anomaly prediction accuracy varies with the threshold value in the same way for the two network models. In order to confirm the threshold of 0.63 is valid in all cases, we need to do some more

investigations. However, at least it indicates that the difference of sensitivity of different satellites may be accounted for by changing the value of the threshold.

Table 9. One day ahead prediction accuracy on Tele-X from Kp (TDNN) vs threshold value.

8	8	0.40	0.635	0.898	0.300
8	8	0.50	0.635	0.784	0.457
8	8	0.55	0.635	0.743	0.529
8	8	0.60	0.635	0.701	0.586
8	8	0.65	0.635	0.653	0.707
8	8	0.70	0.635	0.599	0.771
8	16	0.40	0.642	0.880	0.307
8	16	0.50	0.642	0.796	0.457
8	16	0.55	0.642	0.760	0.529
8	16	0.60	0.642	0.701	0.600
8	16	0.65	0.642	0.635	0.700
8	16	0.70	0.642	0.581	0.764

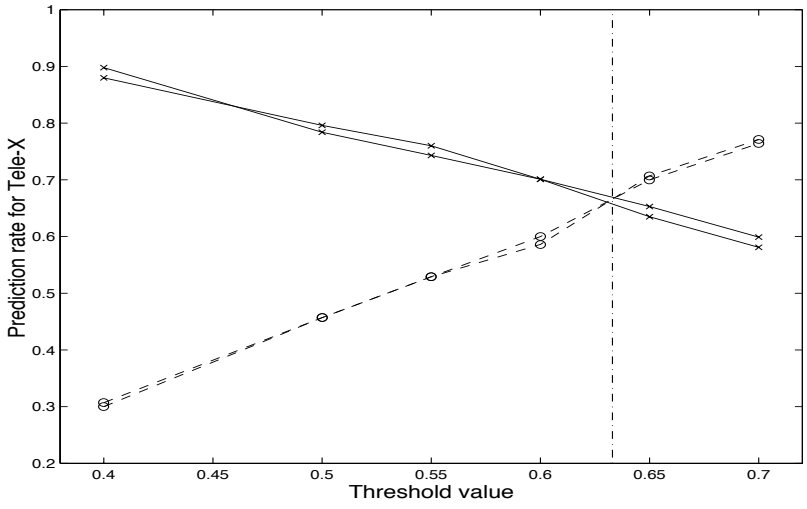

Figure 8. *The prediction accuracy for Tele-X versus the threshold value. The solid line represents the prediction for anomalies on Tele-X and the dashed line represents the prediction for non-anomalies on Tele-X.*

6 Summary and conclusions

Relationship between geostationary spacecraft anomalies and geomagnetic or orbit averaged environment parameters were investigated through superposed epoch analysis and neural network models. The main results are summarised below.

6.1 Superposed epoch analysis

We found from the superposed epoch analysis that:

- The spacecraft anomalies frequently occurred during the recovery phase of geomagnetic storm;
- The space environment conditions during the last 4 - 6 days preceding an anomaly contribute statistically the most to the anomaly occurrence;
- Kp and Dst are better parameters than the relativistic electron flux to predict anomalies on Meteosat-3, suggesting that the anomalies on Meteosat-3 were mainly caused by electrons with energy well below 2 MeV (several keV to 300 keV) via, e.g., surface charging or internal charging;

6.2 Neural network predictions

We find from TDNN predictions that for Meteosat-3 daily-summed Kp, daily-averaged Dst, and daily-averaged energetic electron flux give the total prediction rate of 79%, 73%, and 62%, respectively. For Tele-X, Kp, Dst and energetic electron flux gives the total prediction rate of 64%, 66%, and 67%, respectively. The prediction results from LVQ are similar to those given by TDNN.

The prediction results are consistent with the superposed epoch analysis in terms of correlation with environment parameters. The developed NN models can be used to forecast days with higher risks for anomalies using ACE solar wind data or from real-time estimate of Kp.

6.3 Threshold value and satellites

In order to investigate difference of susceptibility to the space environment for Meteosat and Tele-X, we studied how the threshold value affects the prediction accuracy for anomalies and non-anomalies. For the two types of neural networks trained on Meteosat-3 anomaly data, we have found that a new threshold value can improve the predictions of Tele-X anomalies giving a prediction rate of about 65 percent for both anomalies and non-anomalies on Tele-X. This indicates that despite difference of susceptibility between different spacecraft similar

non-linear methods can be used to predict their anomalies provided a slight change of one parameter

6.4 Future work

Finally we have the following suggestions for the future work:

- Analyse and model on higher time resolution, therefore more local space environment conditions can be taken into account;
- Use other global geomagnetic indices like am or Km and substorm indices (e.g., AE); [Menvielle and Berthelier, 1991];
- Use lower energy electron flux to better capture the anomalies involving surface charging.

7 Acknowledgements

We wish to thank the ESA-TOS-EMA for initiating this project and their interest throughout its completion. Special thanks belong to the ESTEC Technical Officer Dr. Alain Hilgers and to Dr. Eamonn Daly whose comments and support were particularly useful.

8 References

Andersson, L., L. Eliasson, J.G. Wu, H. Lundstedt, Study of Plasma and Energetic Electron Environment and Effects - Spacecraft Anomaly Forecasting Using Heterogenous Environment Data, Technical Note WP 230 ESTEC/Contract No. 11974/96/NL/JG(SC), 1999.

Bartels, J., The standardized index, Ks, and the planetary index. Kp, IATME Bull. 12b, 97, IUGG Pub. Office, Paris, 1949.

Hertz, J., A. Krogh and R. G. Palmer, Introduction to the theory of neural computation, ch. 6, Addison-Wesley, 1991.

Hilgers, A., D. Grystad, L. Andersson, and J.-G. Wu, Prediction of Meteosat anomalies based on space weather, WPP-ISS, pp. 297-300, ESTEC, Noordwijk, The Netherlands, 1998.

Joselyn, J.A., Geomagnetic activity forecasting: The state of the art, Rev. of Geophys., 33 (3), 383, 1995.

Koons, H.C., and D.J. Gorney, A neural network model of the relativistic electron flux at geosynchronous orbit, J. Geophys. Res., 96, 5549, 1991.

Lòpez Honrubia, F.J., A. Hilgers, Some correlation techniques for environmentally induced spacecraft anomalies analysis, J. Spacecraft and Rockets, 34, 670, 1997.

Mayaud, P.N., (eds.), Derivation, meaning, and use of geomagnetic indices, Geophys. Monogr. Ser., vol. 22, AGU, Washington, D.C., 1980.

Menvielle, M., and A. Berthelier, The K-derived planetary indices: Description and availability, Rev. Geophys., 29, 415, 1991.

Nagai, T., Space weather forecast: Prediction of relativistic electron intensity at geosynchronous orbit, Geophys. Res. Lett., 15, 425, 1988.

Rostoker, G., Geomagnetic indices, Rev. Geophys. Space Phys., 10, 935, 1972.

Tribble, A.C., The Space environment: Implications for spacecraft design, Princeton University Press, 1995.

Sugiura, M., Hourly values of equatorial Dst for the IGY, Ann. Int. Geophys. Year, 35, 1964.

Vampola, A.L., Thick dielectric charging on high-altitude spacecraft, J. Electrost., 20, 21, 1987.

Vampola, A.L., Analysis of environmentally induced spacecraft anomalies, J. Spacecraft and Rockets, 31, 154, 1994.

Wrenn, G.L., Conclusive evidence for internal dielectric charging anomalies on geosynchronous communications spacecraft, J. Spacecraft and Rockets, 32, 514, 1995.

Wu, J.-G., and H. Lundstedt, Prediction of geomagnetic storms from solar wind data using Elman recurrent neural networks, Geophys. Res. Lett., 319, 1996.

Wu, J.-G., and H. Lundstedt, Geomagnetic storm forecast from solar wind data with the use of dynamic neural networks, J. Geophys. Res., 102, 14255-14268, 1997a.

Wu, J.-G., and H. Lundstedt, Neural network modeling of solar wind-magnetosphere interaction, J. Geophys. Res., 102, 14457-14466, 1997b.

Wu, J.-G., H. Lundstedt, P. Wintoft, and T.R. Detman, Neural network models predicting the magnetospheric response to the 1997 January halo-CME event, Geophys. Res. Lett, 25, 3031-3034, 1998.

Institutet för rymdfysik

Swedish Institute of Space Physics

Swedish Institute of Space Physics
Box 812, SE- 981 28 Kiruna, SWEDEN
tel. +46-980-790 00, fax +46-980-790 50, e-post: irf@irf.se

www.irf.se